Characterization of deformation bands associated with normal and reverse stress states in the Navajo Sandstone, Utah

John G. Solum, J. P. Brandenburg, Stephen J. Naruk, Olga V. Kostenko, Scott J. Wilkins, and Richard A. Schultz

ABSTRACT

Deformation-band networks at Buckskin Gulch, Utah, and the Big Hole fault, Utah, both formed in the Navajo Sandstone with similar initial porosity and permeability, at similar burial depths, and result in similar reductions in effective permeability. However, the band networks at Buckskin Gulch, which formed in a contractional tectonic setting, appear to be much more areally extensive and are not associated with any discrete faults having displacements greater than at most a few meters and more likely only a few tens of centimeters. In contrast, the bands at Big Hole fault are generally limited to the damage zone of a about 25-m (82-ft) displacement normal fault formed in a locally extensional environment. These results suggest that deformation bands in well core from extensional settings may be indicative of discrete damage zones associated with normal faults, whereas deformation bands in well core from contractional settings may be indicative of much more areally extensive deformation-band networks. The band networks in both cases will affect similar reductions in reservoir effective permeability, but only in the latter case will the affected area be sufficiently large to affect well performance.

INTRODUCTION

Coarse, well-sorted sandstone with high porosity and quartz content is close to an optimal reservoir material. However, such sandstones may deform by unique mechanisms that make reservoir forecasting more challenging, that is, the formation of

Manuscript received August 5, 2009; provisional acceptance September 23, 2009; revised manuscript received December 14, 2009; final acceptance January 5, 2010.
DOI:10.1306/01051009137

AUTHORS

JOHN G. SOLUM ~ *Shell International Exploration and Production, Inc., Bellaire Technology Center, Houston, Texas; j.solum@shell.com*

John Solum is a structural geologist with the Clastics Reservoir Research Team at Shell International Exploration and Production. He received his B.S. degree in geology from Utah State University (1998) and his M.S. degree (2001) and Ph.D. (2005) from the University of Michigan. Prior to joining Shell in 2007, he was on the faculty at Sam Houston State University in Huntsville, Texas (2006–2007), and a Mendenhall Fellow at the U.S. Geological Survey in Menlo Park, California (2005–2007).

J. P. BRANDENBURG ~ *Shell International Exploration and Production, Inc., Bellaire Technology Center, Houston, Texas*

J. P. Brandenburg received his B.S. degree in geology from Michigan State University in 2000 and his Ph.D. in geology from the University of Michigan in 2008. He is currently employed as a research geologist by Shell Upstream Projects and Technology in Houston, Texas. He specializes in numerical modeling techniques for geology.

STEPHEN J. NARUK ~ *Shell International Exploration and Production, Inc., Bellaire Technology Center, Houston, Texas*

Stephen Naruk has more than 20 years of experience with Shell, in multiple exploration and production and research and development assignments. He is currently a principal structural geologist and leads both Shell's Clastics Reservoir Research Team and the Structural Geology Center of Expertise within Shell's Expertise and Deployment organization.

OLGA V. KOSTENKO ~ *Shell International Exploration and Production, Inc, Bellaire Technology Center, Houston, Texas*

Olga V. Kostenko is a production geologist with the Perdido deep-water venture. She is involved in drilling operations, reservoir modeling, and structural evaluation of near-field exploration opportunities. She received her geological engineering degree from Kyiv State University, Ukraine, and her Ph.D. in geology from the University of Oslo, Norway (2002). Prior to joining Shell, she was a project geoscientist for exploration and research projects in Canada, Ukraine, Russia, and Kazakhstan while working for small independent

oil and gas companies. Her previous assignment with Shell (2005–2008) was with the Novel Appraisal Technology Team in Shell International Exploration and Production. She held the position of structural geologist and was involved in research projects and global technical consulting to asset teams mainly in the fields of structural modeling and trap analysis.

SCOTT J. WILKINS ~ *Shell International Exploration and Production, Inc., Bellaire Technology Center, Houston, Texas; present address: Anadarko Petroleum Corporation, The Woodlands, Texas*

Scott Wilkins is a structural geologist within the Geoscience Technology group at Anadarko Petroleum Corporation. His current work involves global technical support for exploration and production, focusing on fault seal analysis, fracture characterization, rock mechanics, and seismic interpretation. He was previously in a similar role, as well as New Ventures Exploration, at Shell International E&P (2002–2008). He received his M.S. degree from Florida International University in 1999 and Ph.D. from the University of Nevada, Reno, in 2002.

RICHARD A. SCHULTZ ~ *Geomechanics-Rock Fracture Group, Department of Geological Sciences and Engineering, University of Nevada, Reno, Nevada*

Richard Schultz received his B.A. degree in geology from Rutgers University (1979), his M.S. degree in geology from Arizona State University (1982), and his Ph.D. in geomechanics and structural geology from Purdue University (1987). Since joining the University of Nevada, Reno, in 1990 he has worked in rock fracture and rock mass mechanics, growth and scaling of fractures and deformation bands, and development of deformation-band damage zones and compaction bands.

ACKNOWLEDGEMENTS

The authors thank Shell International Exploration and Production for the permission to publish the results of this study and George Davis, Steve Hansen, and an anonymous reviewer for constructive reviews of this manuscript. Lori Hathon and Tim Diggs are thanked for their help with the collection of the photomicrographs.

The AAPG Editor thanks the following reviewers for their work on this article: George H. Davis, Steve Hansen, and an anonymous reviewer.

deformation bands (Fossen et al., 2007; Schultz and Fossen, 2008). Deformation bands are essentially faults or shear zones in weakly consolidated to unconsolidated granular material. More specifically, deformation bands are zones of localized grain rearrangement (packing geometry, rotation, and sliding) and cataclasis (breaking, spalling, and crushing) developed to varying extents, typically on the order of a few host-rock grain diameters in thickness (e.g., Aydin, 1978; Pittman, 1981; Aydin and Johnson, 1983). Compaction bands are a type of deformation band that accommodates closing displacements, including porosity loss caused by grain reorganization and/or cracking, with no shearing within the band (Mollema and Antonellini, 1996; Sternlof et al., 2005; Schultz and Fossen, 2008). Deformation-band arrays are common as dense arrays in the damage zones of faults cutting sandstone but can also be distributed between fault zones and related to regional deformation. Regardless of their type, deformation bands typically have a lower permeability than their undeformed host rocks. Where present in small numbers, they have little or no effect on reservoir performance. However, where present in large numbers, they can significantly reduce reservoirs' effective permeabilities and hence well performance (e.g., Myers, 1999; Shipton et al., 2002; Flodin et al., 2005).

Deformation bands are commonly observed in core, and when such observations are made in appraisal settings, predicting both their permeability and their distribution to forecast the effect, if any, on reservoir performance is critical. Specifically, modeling the spatial distribution of deformation bands and their permeabilities allows their effect on bulk permeability to be calculated. This article compares and contrasts two occurrences of deformation bands that formed in the same host-rock unit (Navajo Sandstone) and at similar burial depths and times. The geometric characteristics and permeability reductions of the bands are similar. However, in the first case, a contractional setting (East Kaibab monocline), the bands occur over a sufficiently large area to degrade well performance. In the second case, an extensional setting (Big Hole fault), the bands appear limited to the damage zone of a normal fault and do not occur over a sufficiently large area to adversely affect well performance. In the second case, the bands appear to have formed under significantly less mean effective stress than in the first case. We infer that this difference between tectonic environments and associated stresses is a primary criterion for identifying when deformation bands potentially occur in sufficient numbers to degrade reservoir performance.

Deformation bands have been documented in sandstones of virtually every provenance in both the field and subsurface.

Table 1. Definitions of Types of Deformation Bands Described in This Study*

Deformation band	Generic term covering any thin, tabular zone of deformation. Includes shear bands, noncataclastic shear bands, and compaction bands.
Shear band	A deformation band that accommodates shear offset, dominantly through cataclasis. Observed at Buckskin Gulch and the Big Hole fault.
Shear band fault	A fault composed of a coalescence or amalgamation of shear bands.
Noncataclastic shear band	A shear band that accommodates offset with little observable cataclasis. Inferred to form early in burial history at shallow depths. Observed at the Big Hole fault.
Compaction band	A deformation band without shear offset that accommodates negative elongation through grain packing and reorganization. Observed at Buckskin Gulch.

*Dilational bands are reported in the literature but are not observed at either Buckskin Gulch or the Big Hole fault.

For example, deformation bands have been described in fluvial sands (Parnell et al., 2004), deltaic sands (Gibson, 1994), and near-shore marine sands (Cashman and Cashman, 2000). Deformation bands are particularly common in deformed eolian sandstone and have been described in multiple locations in the southwestern United States in Utah (Aydin, 1978; Antonellini and Aydin, 1995; Fossen and Hesthammer, 1998; Davis et al., 1999; Shipton et al., 2002; Davatzes et al., 2003; Schultz and Balasko, 2003; Berg and Skar, 2005; Fossen et al., 2005) and Nevada (Myers, 1999; Taylor and Pollard, 2000; Flodin et al., 2003, 2005; Eichubl et al., 2004). Similar surface exposures have also been documented in Scotland (Underhill and Woodcock, 1987; Parnell et al., 2004). For a more comprehensive discussion of deformation-band occurrences, see recent reviews by Aydin et al. (2006) or Fossen et al. (2007). The types of deformation bands observed at Buckskin Gulch and along the Big Hole fault are given in Table 1.

Deformation bands are commonly observed in reservoirs, and there are examples of fields in which deformation bands impact production as well as examples of fields in which deformation bands do not inhibit production. For example, the Gullfaks (Hesthammer et al., 2002) and Huldra (Fossen et al., 2003) fields in the North Sea Brent province contain deformation bands, but they have little effect on well communication. In contrast, the Gullfaks Sør field in the North Sea Brent province (Hesthammer et al., 2002) and the Ganymede field in the Rotliegendes (Leveille et al., 1997) contain faults and deformation bands that baffle flow and enhance fault seal. In the case of the Gullfaks Sør field, the actual production was only 15% of the anticipated production (Hesthammer et al., 2002). Although all of the abovementioned fields are lithologically similar, the Gullfaks Sør and Ganymede fields are hotter and experienced significant quartz cementation, which made the deformation bands in those fields relatively tight. Without that cementation, the deformation bands in the Gullfaks Sør and Ganymede likely would not have negatively impacted reservoir performance.

Examples of reservoirs with noncemented bands still baffle flow. The Arroyo Grande field in the marine Miocene–Pliocence Pismo Formation in California contains zone deformation bands that contain tar on one side but not on the other (Antonellini et al., 1999). Steam conductivity in that field was nine times higher parallel to the deformation bands than perpendicular to them, indicating that the band arrays and associated faults controlled the steam flood (Antonellini et al., 1999). The Anschutz Ranch East field in the Nugget Sandstone (equivalent to the Navajo) in Wyoming is a fault-related anticline that contains many deformation bands observed in the core (Lewis and Couples, 1993). In places, these bands separate bitumen-stained and clean sandstones, similar to the Arroyo Grande field, providing an indication of baffling. The bands at the Anschutz Ranch East field are interpreted to occur over a large area in the hinge of the fold. This is an indication that deformation bands can degrade reservoir permeabilities over areas that are large enough to impair well performance.

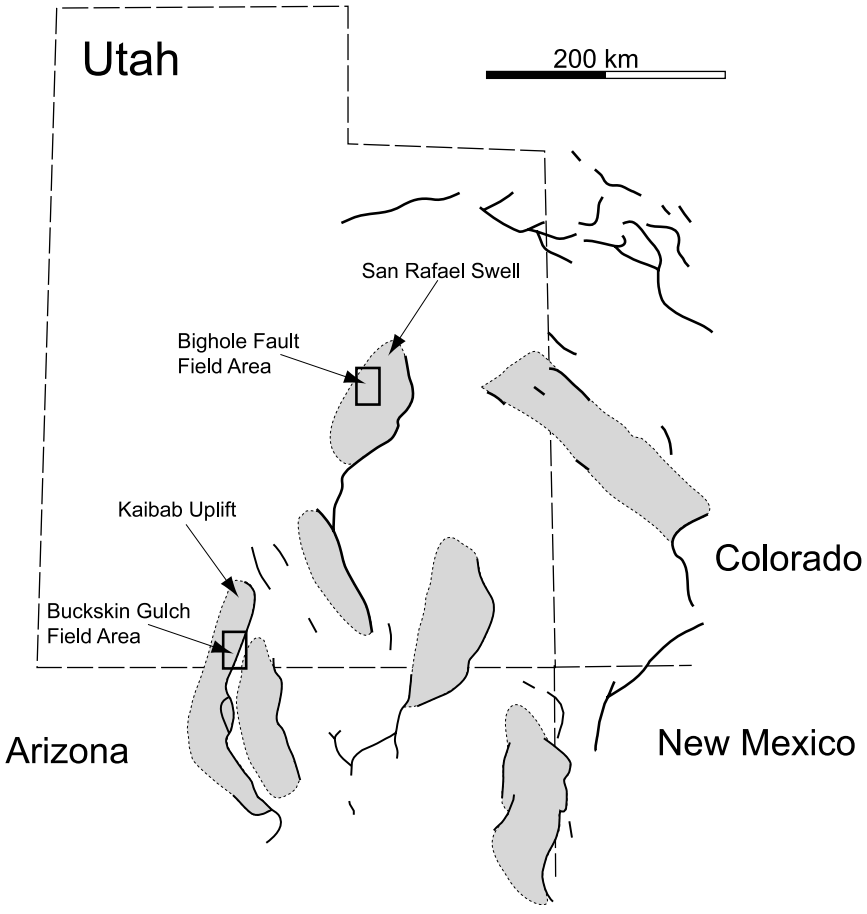

Figure 1. Locations of the Big Hole fault and Buckskin Gulch field areas relative to major monoclines (heavy lines) and related uplifts (shaded) of the Colorado Plateau. Redrawn from Davis (1978).

One major difference between the group of fields that were affected by deformation bands and the group that was not is the stress state. The Gullfaks and Huldra fields occur in a normal-faulting environment, whereas the Arroyo Grande and Anschutz Ranch East fields occur in a reverse-faulting environment. The goal of this report is to determine the function of stress state in the development of deformation-band networks because it appears that some aspect of a reverse-faulting environment (likely higher mean stress) promotes the formation of features that cause compartmentalization.

The preservation and exposure of these deformation-band networks in some outcrops are so complete that several workers have used spatial characteristics measured in these exposures as the quantitative basis for modeling deformation bands in the subsurface. Such research is ongoing and has yielded a wealth of information, particularly in terms of characterizing deformation bands in the damage zones of faults (Antonellini and Aydin, 1994, 1995; Fowles and Burley, 1994; Knott et al., 1996; Beach et al., 1999; Shipton and Cowie, 2001; Du Bernard et al., 2002; Shipton et al., 2002, 2005; Berg and Skar, 2005; Fossen et al., 2007). Here, we contribute to this effort by presenting a comparison of deformation bands at the Big Hole fault and Buckskin Gulch sites in southern Utah (Figure 1). Both sites contain exposures of extensive deformation-band networks developed in response to Laramide deformation of the Colorado Plateau. However, they differ in terms of mode of deformation. At the Big Hole fault, deformation bands occur primarily but not exclusively in the damage zone of a large normal fault with a throw of up to approximately 24 m (79 ft) (Shipton and Cowie, 2001; Shipton et al., 2002, 2005). Deformation bands at Buckskin Gulch are more areally extensive and related to thrusting associated with the development of the east Kaibab monocline (Mollema, 1994; Mollema and Antonellini, 1996; Davis, 1999; Schultz, 2009; Tindall and Davis, 1999).

GEOLOGIC SETTING

The two field sites represented in this study were chosen because of the commonality of stratigraphic unit (Navajo Sandstone) as well as the timing of driving forces for deformation-band formation (Laramide deformation of the Colorado Plateau). Figure 1 illustrates the relationship of both field sites to the principal uplifts and monoclines of the Colorado Plateau. Although debate about the causes of mechanisms of uplift in this region is ongoing, these monoclines are generally accepted as Laramide structures associated with the reactivation of high-angle Precambrian normal faults during the Cretaceous and Tertiary (e.g., Davis, 1978). Both the Buckskin Gulch and Big Hole fault field locations contain excellent exposure of the eolian Navajo Sandstone with extensive populations of deformation bands. The Navajo Formation is Jurassic in age, with somewhat uncertain age relationships to underlying strata (Marzolf, 1983). Overall sedimentary thickness increases, and the formation becomes increasingly sand rich from the northeast to the southwest (Marzolf, 1983; Beitler et al., 2005). The Navajo Sandstone is stratigraphically equivalent to the Aztec Sandstone in Nevada (Marzolf, 1983), which also hosts numerous deformation bands in the Valley of Fire State Park (e.g., Taylor and Pollard, 2000; Flodin et al., 2003; Sternlof et al., 2005). The depositional history of the Navajo and related sandstones is summarized by Dickinson and Gehrels (2009).

Buckskin Gulch

Several authors have extensively characterized deformation bands in the Navajo Sandstone deformed in association with the formation of the East Kaibab monocline (Mollema and Antonellini, 1996; Davis, 1999; Davis et al., 1999; Tindall and Davis, 1999). Most of these studies focused on deformation bands to the north of Highway 89 where the hinge zone of the monocline is well exposed (e.g., Tindall and Davis, 1999). However, the Buckskin Gulch field location (Figure 2) is uniquely situated in approximately flat-lying strata to the east of the forelimb (Mollema and Antonellini, 1996). Because of the northward plunge of the anticline (Doelling and Davis, 1989), exposure of the Navajo Sandstone expands from north to south and is marked by extensive lateral exposure in the Buckskin Gulch proper. This location is marked by a distinctive topography of ridge tops capped by flat zones of coalesced shear bands (deformation-band faults) that are particularly resistant to weathering (similar to the flying pancakes of Davis, 1999). In addition to providing a unique view of deformed Navajo Sandstone, Buckskin Gulch is one of only two field locations (the other being Valley of Fire in Nevada) where compaction bands have been documented. Buckskin Gulch is located at the eastern edge of the Kaibab uplift. Although a pretectonic, noncataclastic population has been proposed (Davis, 1999), most of the deformation bands at this location are related to the growth of the East Kaibab monocline (Mollema and Antonellini, 1996). Tindall and Davis (1999) suggested that growth of the monocline may have involved a significant component of strike-slip motion. However, the deformation bands at Buckskin Gulch show predominantly reverse offsets. This kinematic sense is supported by the orientation of a conjugate set of deformation-band shear zones and compaction bands relative to the strike of the monocline (Mollema and Antonellini, 1996) indicating a thrust-faulting tectonic environment. Davis (1999) reported that structures associated with the East Kaibab monocline deform the Cretaceous Straight Cliffs Formation, and based on the mapping of Doelling and Davis (1989), strata as young as the Kaiparowits Formation are deformed. Based on palynology, the Straight Cliffs Formation is Turonian to Santonian (Nichols, 1997), whereas the Kaiparowits Formation is Campanian (Cifelli, 1990). These ages indicate that the monocline was active as young as 89–71 Ma. The deformation-band arrays at Buckskin Gulch are similar to an exposure in the Valley of Fire in southern Nevada that formed during the Sevier orogeny. Ash beds underlying synorogenic sediments at the Valley of Fire have been dated to about 98–102 Ma (Bohannon, 1983; Troyer et al., 2006), providing a lower limit on the age of band formation at that location. Assuming that the Buckskin Gulch and Valley of Fire band arrays formed coevally and adding in

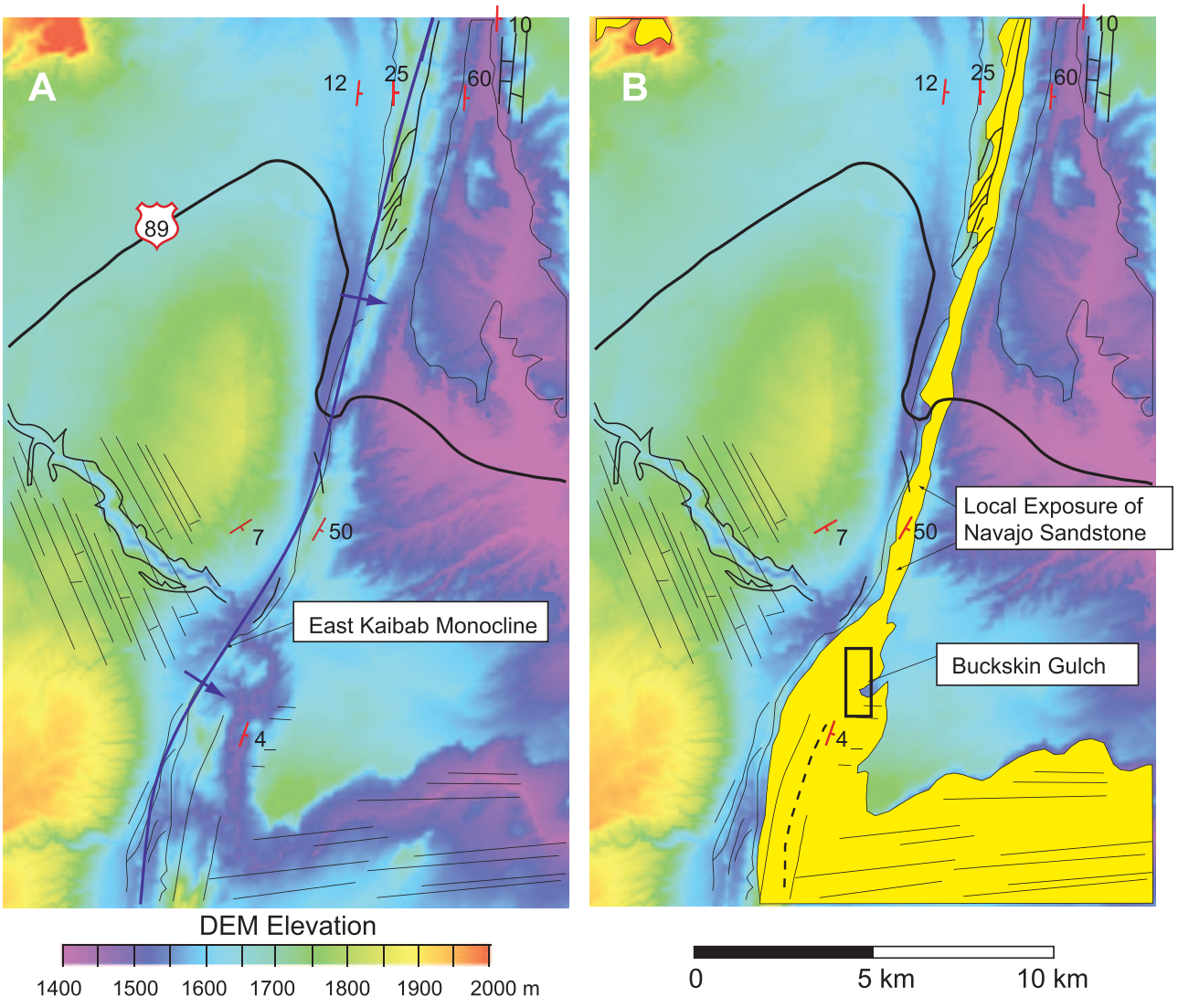

Figure 2. Buckskin Gulch field area and vicinity. The digital elevation map (DEM) was generated from a 5-m (16-ft) vertical resolution light detection and ranging (LIDAR) from the Utah State Geographic Information Database. The superimposed geologic map was redrawn from Mollema and Antonellini (1996). Panel A highlights structural features; panel B highlights the regional surface exposure of the Navajo Sandstone and the location where measurements were taken (Buckskin Gulch). The hinge of the monocline is drawn based on the inference of the authors. Thin lines are joints mapped in the original figure.

the stratigraphic constraints on the age of the East Kaibab monocline, the deformation-band arrays at Buckskin Gulch formed between 71 and 102 Ma.

Using the stratigraphic thicknesses given by Davis (1999), the Buckskin Gulch Band arrays formed at a depth of about 1.5–3 km (0.9–1.8 mi).

Big Hole Fault

The Big Hole fault field location is situated approximately 250 km (155 mi) to the north-northwest of Buckskin Gulch, near a prominent knob known as Chimney Rock (Figure 3), the namesake of the Chimney Rock fault array (Krantz, 1988). Here, the capping Carmel Formation has proven more resistant to weathering, exposing the Navajo Sandstone primarily along dry gullies (Witkind, 1988). The Chimney Rock fault network comprises a system of small normal faults. Deformation bands (shear bands) in the damage zone of the larger Blueberry fault and Big Hole fault have been the basis for prior spatial analysis (Shipton and Cowie, 2001; Shipton et al., 2002) and behind-outcrop

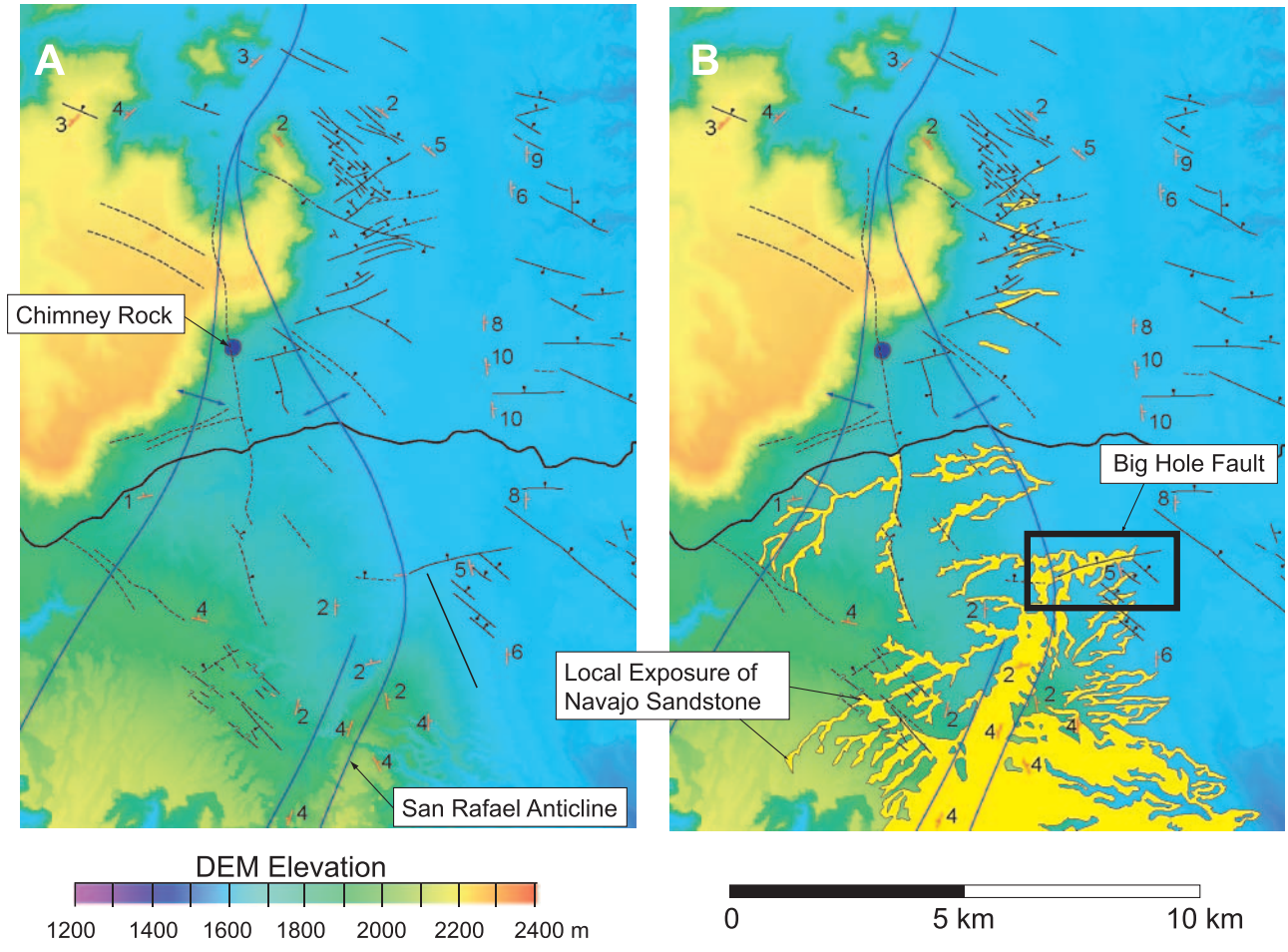

Figure 3. Big Hole fault field area and vicinity. The digital elevation map (DEM) was generated from a light detection and ranging (LIDAR) from the Utah State Geographic Information Database. The superimposed geologic map was redrawn from Witkind (1988). Panel A highlights structural features; panel B highlights the regional surface exposure of the Navajo Sandstone and the location where measurements were taken along the Big Hole fault. Thin lines and dashed lines are faults.

drill-core studies (Shipton et al., 2005). Although extensive deformation-band networks are readily spotted in outcrop, the deformation-band-controlled geomorphology that is so prominent at Buckskin Gulch is lacking in this area. No compaction bands have been observed in the vicinity of the Big Hole fault, although two types of shear bands are observed. The first is the cataclastic shear bands described above, whereas the second are darker, noncataclastic bands, which are similar to the subvariety DB2b bands that Davis (1999) reported in the Navajo Sandstone in the southern part of the Colorado Plateau in Utah.

In contrast to the marginal location of Buckskin Gulch, the Big Hole fault location is near the center of the San Rafael swell. Here, uplift-related deformation is expressed as a gentle folding of strata (Witkind, 1988) and by an associated set of small normal faults (the Chimney Rock fault array) in an approximately orthorhombic pattern (Krantz, 1988; Davatzes et al., 2003). Observations from both locations can be treated as different facets of deformation from the same larger scale tectonic event (i.e., Laramide deformation of the Colorado Plateau; Engebretson et al., 1984). Although a specific relationship has not been established, this fault array likely formed in response to flexure of the San Rafael swell at approximately 58–79 Ma (Shipton et al., 2002). Shipton and Cowie (2001) estimated that the Big Hole fault was active at a depth of 1.5–3 km

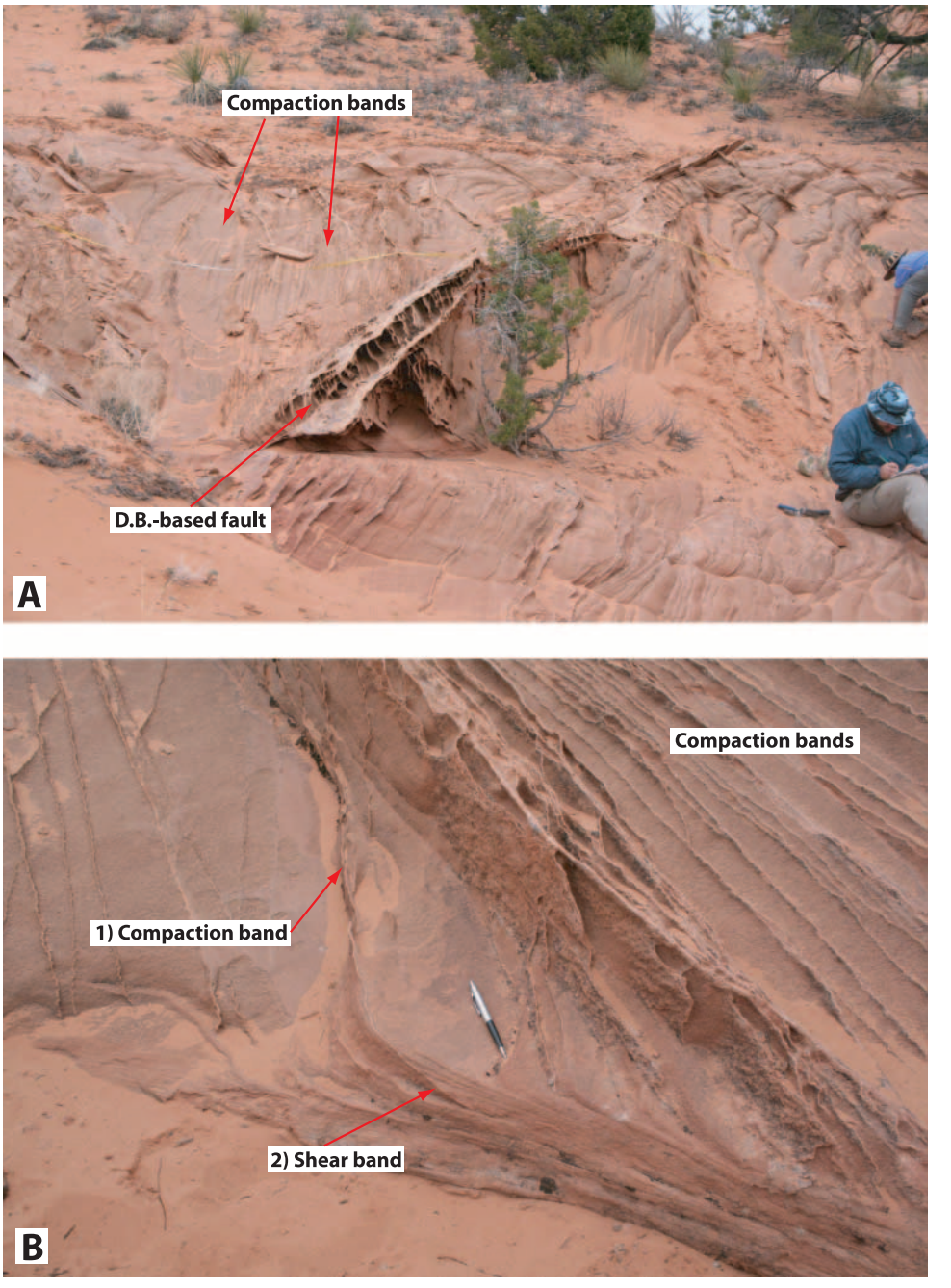

Figure 4. Outcrop photos of deformation-band occurrences at Buckskin Gulch. (A) Overview of the scan-line location showing compaction bands and one deformation (shear) band (D.B.)-based fault. (B) View of the compaction band changing into a shear band near a dune boundary. This change indicates that the shear and compaction bands are coeval at this location.

(0.9–1.8 mi), which is similar to the depth estimates for Buckskin Gulch.

BAND DATA

One scan line oriented perpendicular to the strike of the deformation bands noting deformation-band thickness, orientation, and position was collected at each field site. Overview photographs of the scan lines are shown in Figures 4 and 5. The scan line at Buckskin Gulch crosses two deformation (shear)-band faults; defined by coalescences of shear bands, but lacking a thoroughgoing slip surface, and therefore accommodating little displacement using the model of deformation-band fault formation described by Aydin (1978). Similarly, the scan line at Big Hole crosses two normal faults, one with a 3-m (10-ft) throw, the other with 14 m (46 ft). The compaction and shear bands at Buckskin Gulch appear

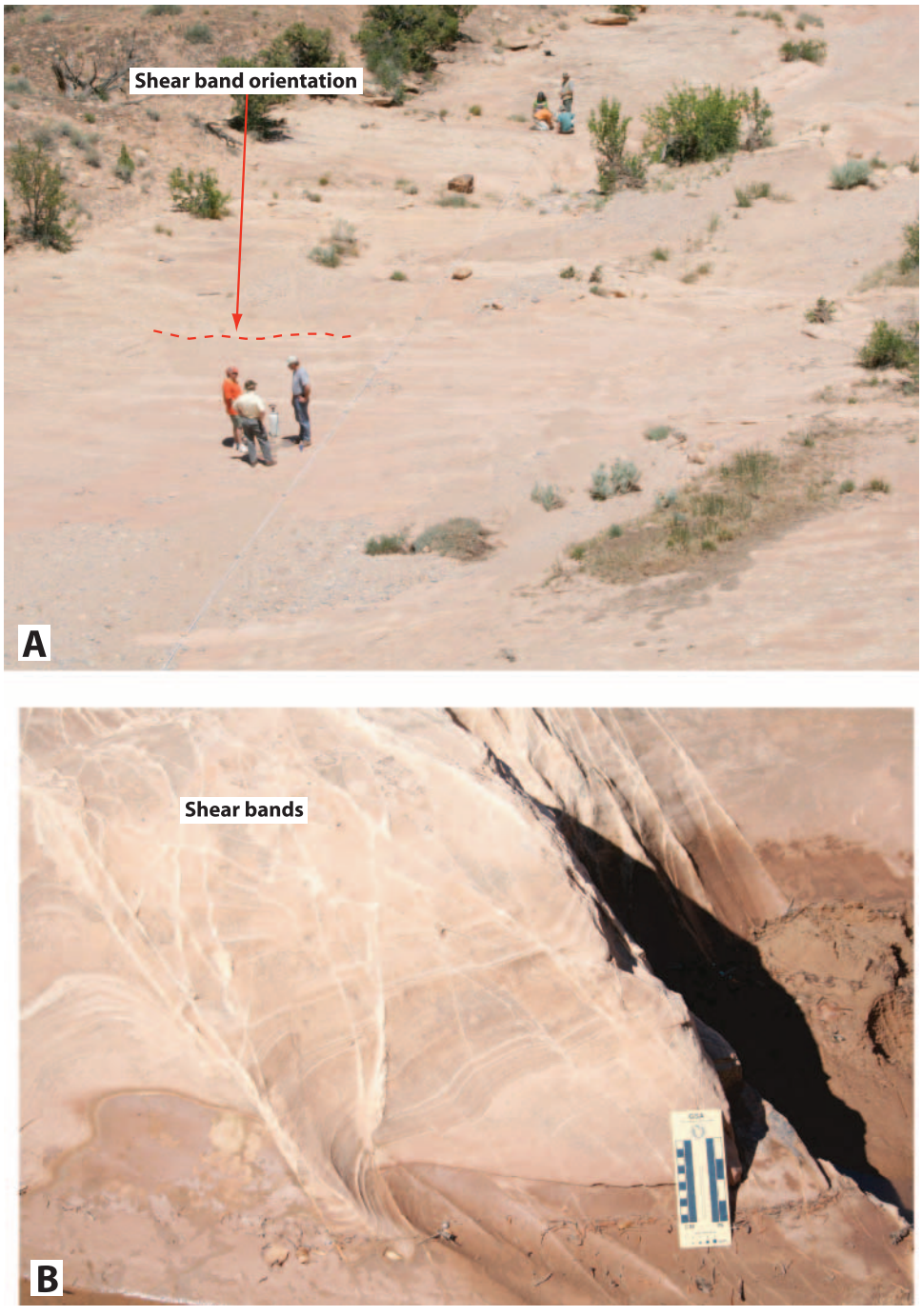

Figure 5. Outcrop photographs of deformation-band occurrences along the Big Hole fault. (A) Overview of the scan line. The general orientation of the deformation bands is given by the dashed line. Most of the lighter colored lineations in that image are deformation bands. (B) Closer view of shear bands along that scan line.

to have formed contemporaneously as indicated by some compaction bands changing to shear bands at dune boundaries (Figure 4B) (Schultz, 2009). Both scan lines cross approximately the same number of bands (~300). Scan-line trajectories were defined using a fiberglass measuring tape, and band thicknesses were measured using a set of calipers. Band orientations were measured when possible.

Band Densities

Band densities for both locations are shown in Figure 6 and listed in Table 2. The average density of bands is greater at Buckskin Gulch (25 bands/m) than at the Big Hole fault (5 bands/m). High band densities (20–25 bands/m or 6–8 bands/ft) at Big Hole are correlated with two normal faults, one with a 3-m (10-ft) throw, the other with a 14-m

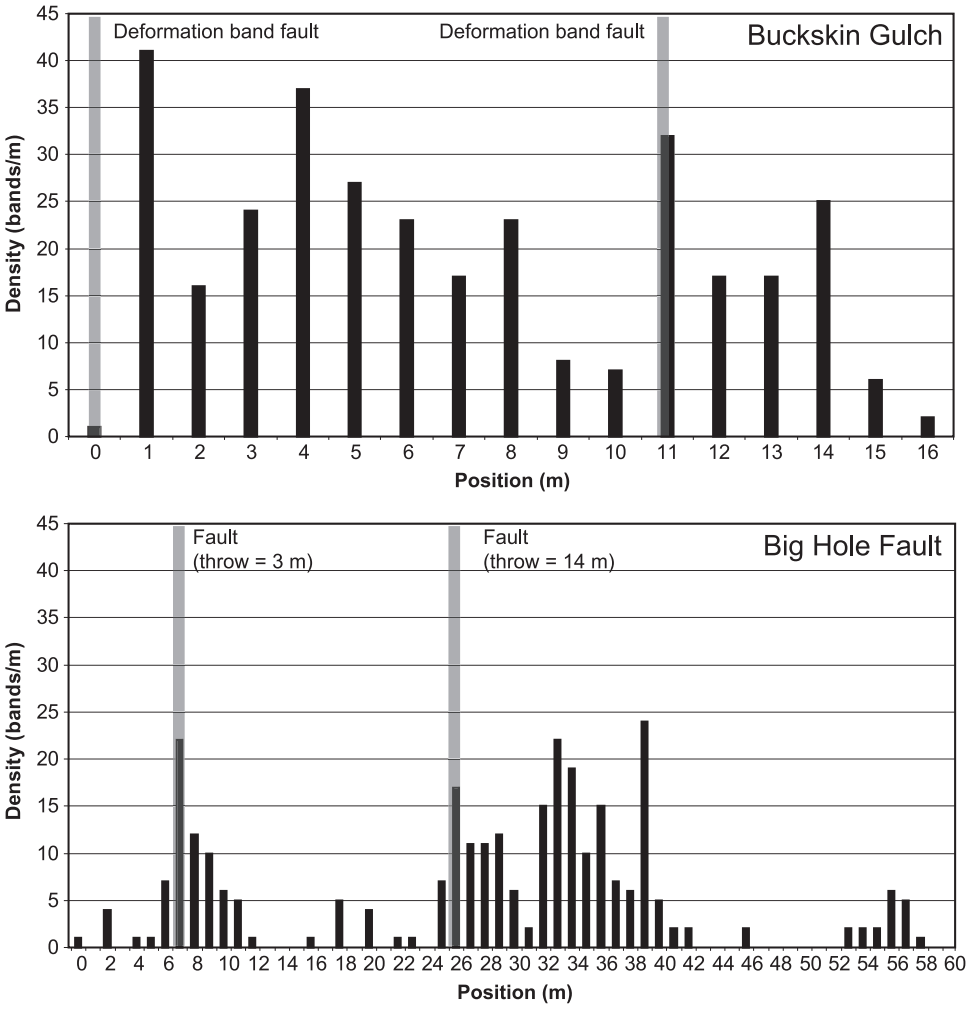

Figure 6. Band densities along the scan lines from Buckskin Gulch and the Big Hole fault.

Table 2. Effective Permeability Calculations for Buckskin Gulch and Big Hole Fault

Buckskin Gulch		Big Hole Fault	
Total scan-line length (ft/m)	50.5/15.4	Total scan-line length (ft/m)	188.3/57.5
Number of bands	315	Number of bands	294
Average band density (#/ft #/m)	7.5/24.6	Average band density (#/ft #/m)	1.6/5.1
Cumulative shear band thickness (ft/m)	0.63/0.19	Cumulative shear band thickness (ft/m)	1.30/0.40
Cumulative compaction band thickness (ft/m)	1.65/0.50	Cumulative noncataclastic band thickness (ft/m)	0.49/0.15
Total band thickness (ft/m)	2.28/0.69	Total band thickness (ft/m)	1.80/0.55
Shear band permeability (low/mean/high) (md)	0.08/0.26/1.16	Shear band permeability (low/mean/high) (md)	0.002/0.13/0.16
Compaction band permeability (low/mean/high) (md)	3.3/39.1/75	Noncataclastic band permeability (low/mean/high) (md)	75/164/285
Host-rock permeability (low/mean/high) (md)	3300/5400/7500	Host-rock permeability (low/mean/high) (md)	660/880/1100
K_{eff} using mean permeabilities (md)	20	K_{eff} using mean permeabilities (md)	18
Mean K_{eff}/mean host-rock permeability	20/5400 = 0.004	Mean K_{eff}/mean host-rock permeability	18/880 = 0.020

(46-ft) throw (Shipton et al., 2002), showing that the high density at that location is correlated with fault damage zones. The greatest band density observed at Big Hole (~25 bands/m or 8 bands/ft) occurs 13 m (43 ft) from the slip surface of a fault with a throw of 14 m (46 ft), although this could be considered part of the damage zone of the Big Hole fault. Bands at Big Hole include white cataclastic bands (268 of 294 bands) and darker noncataclastic bands (26 of 294 bands). Beyond the ends of the scan line, the background density of deformation bands is less than 5/m.

The scan line at Buckskin Gulch crosses two deformation-band faults. The offset along these faults is not known because of the lack of visible offset markers, but because these faults lack throughgoing slip surfaces, they are most likely small displacement features (Aydin, 1978). Cross laminae can be traced across compaction bands, indicating that those features have no offset or at least offset that is below the size of one of the laminae. The band density at Buckskin Gulch shows no clear relationship to these deformation-band faults, indicating they do not control the occurrence of the compaction bands. Twenty-five (of 315) bands were shear bands, whereas 290 of 315 were compaction bands. As mentioned above, both scan lines cross approximately the same total number of bands (315 at Buckskin Gulch vs. 294 at Big Hole).

Band Thicknesses

The mean grain size at Buckskin Gulch in undeformed protolith measured from thin sections is 0.36 mm (0.014 in.), ranging from 0.09 to 0.6 mm (0.004 to 0.024 in.). The mean grain size at the Big Hole fault measured from thin sections is 0.17 mm (0.006 in.), ranging from 0.06 to 0.3 mm (0.002 to 0.012 in.). The band thicknesses at Buckskin Gulch show a skewed normal distribution, with a maximum at 1–2 mm (0.03–0.07 in.) or approximately 3–6 times the mean grain size. Band thicknesses at the Big Hole fault exhibit an exponential distribution with a maximum at the smallest bin size, less than 1 mm (0.03 in.) (Figure 7). Plots of band thickness versus cumulative frequency for Buckskin Gulch and the Big Hole fault differ from one another. As seen on Figure 8, the thickness distributions generally follow a power law distribution, deviating as thickness decreases. The data from Buckskin Gulch deviate from a power law at thickness less than about 1 mm (0.03 in.), whereas the data from the Big Hole fault deviate at about 0.35 mm (0.013 in.). The exponents of the thickness distributions shown on Figure 8 are significantly different for Buckskin Gulch (−1.6) and for Big Hole (−1.0). This slope is a measure of the number of thin bands relative to thick bands. For example, at Buckskin Gulch, the cumulative frequency of 1-mm (0.03-in.)-thick bands is 40 times greater than the cumulative frequency of 10-mm (0.3-in.)-thick bands, whereas that difference is only 10 times at Big Hole.

Spatial Analysis

Scan-line data were also used to calculate the correlation integral (e.g., Du Bernard et al., 2002; Gomez and Marrett, 2007). The correlation integral, also called the correlation sum, is determined by calculating the spacing of every band with respect to every other band in the data set and so provides a more comprehensive determination of the spatial distribution of the bands. Using a slightly modified version of Du Bernard et al. (2002), the correlation sum is given by

$$C_r = \frac{2}{N(N-1)} \sum_{i=1}^{N} \sum_{j=i+1}^{N} \Theta\left[r - (x_j - x_i)\right] \quad (1)$$

where C_r is the correlation sum at a given length scale, r; N is the total number of deformation bands; Θ is the Heaviside step function (0 for $r \leq$ band spacing, and 1 for $r >$ band spacing); and x_j–x_i is the spacing between the centers of the jth and ith bands.

As shown on Figure 9, the exponents of the spacing distributions are very similar at both sites, 0.95 at Big Hole and 0.92 at Buckskin Gulch. Despite this similarity, significant differences in the spatial distributions between the two sites are observed as indicated by the degree of deviation from a random spacing distribution (the red line on Figure 9). Following the method of Gomez and

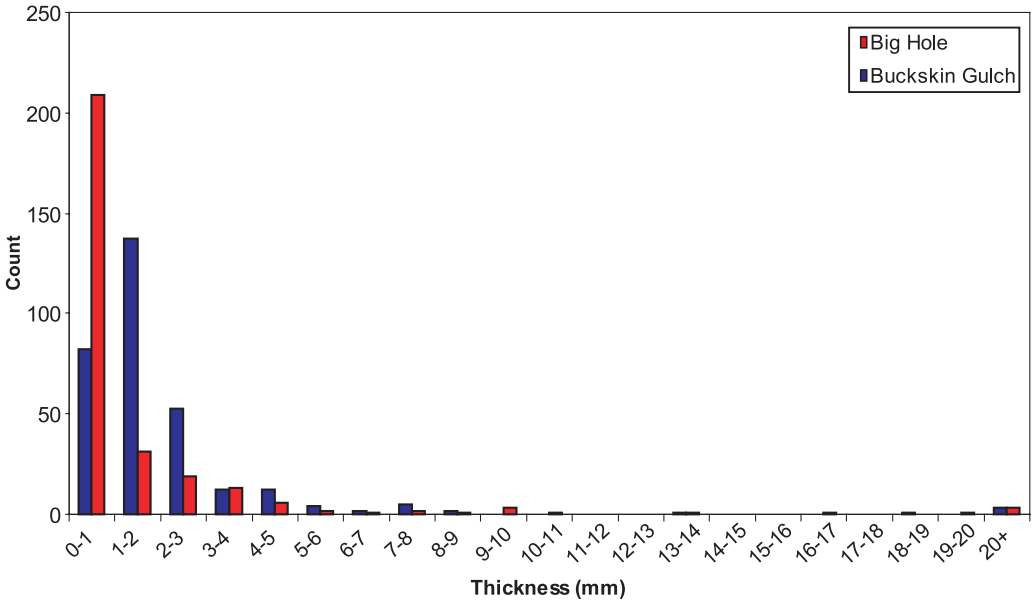

Figure 7. Histogram of band thicknesses for Buckskin Gulch and the Big Hole fault.

Marrett (2007), the observed values are normalized against expected values for a random distribution, which would have a slope of 1 (Du Bernard et al., 2002) (Figure 9). This normalization helps to highlight length scales over which the distribution most deviates from a random distribution. The presence of clusters at both locations is indicated by the normalized data, which have maximum length scale values of about 0.1 m (0.3 ft), and decay exponentially at values greater than 0.1 m (0.3 ft). The point at which these distributions reach a normalized correlation sum of 1 gives the spacing of the clusters (Gomez and Marrett, 2007). The spatial distribution at Buckskin Gulch is close to random, with weakly defined clusters with a spacing of about 2.5 m (8.2 ft). The distribution at Big Hole is much more nonrandom because most of the normalized data have a value greater than 1, with the bands occurring in fractal clusters with a spacing of about 18 m (59 ft).

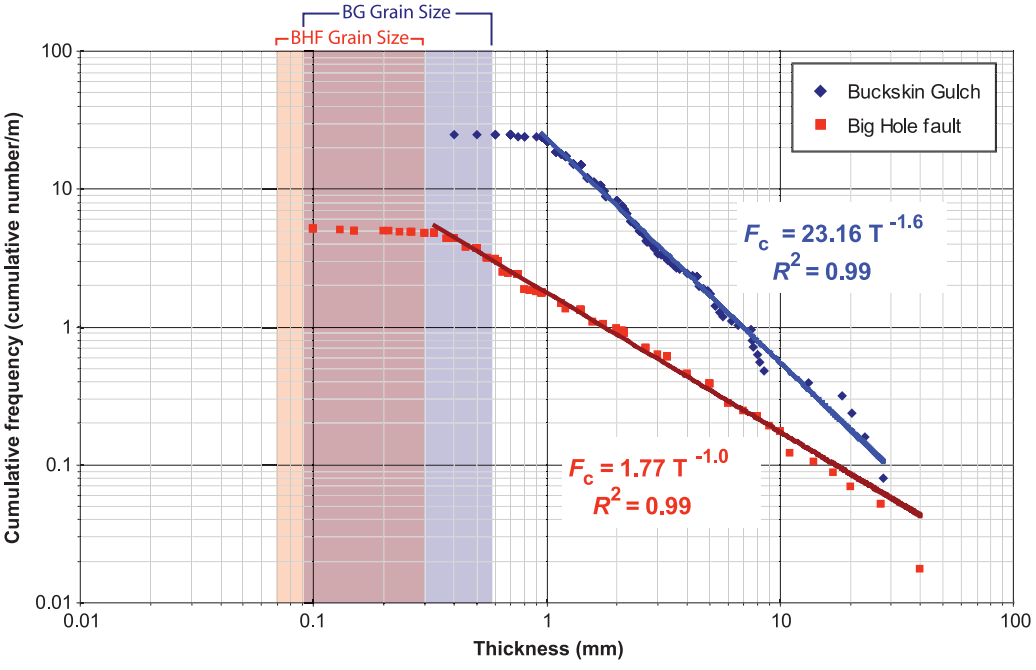

Figure 8. Plot of cumulative frequency (F_c) vs. thickness (T) for deformation bands from both locations. The range of grain sizes from each location is given by the shaded region. BG = Buckskin Gulch; BHF = Big Hole fault.

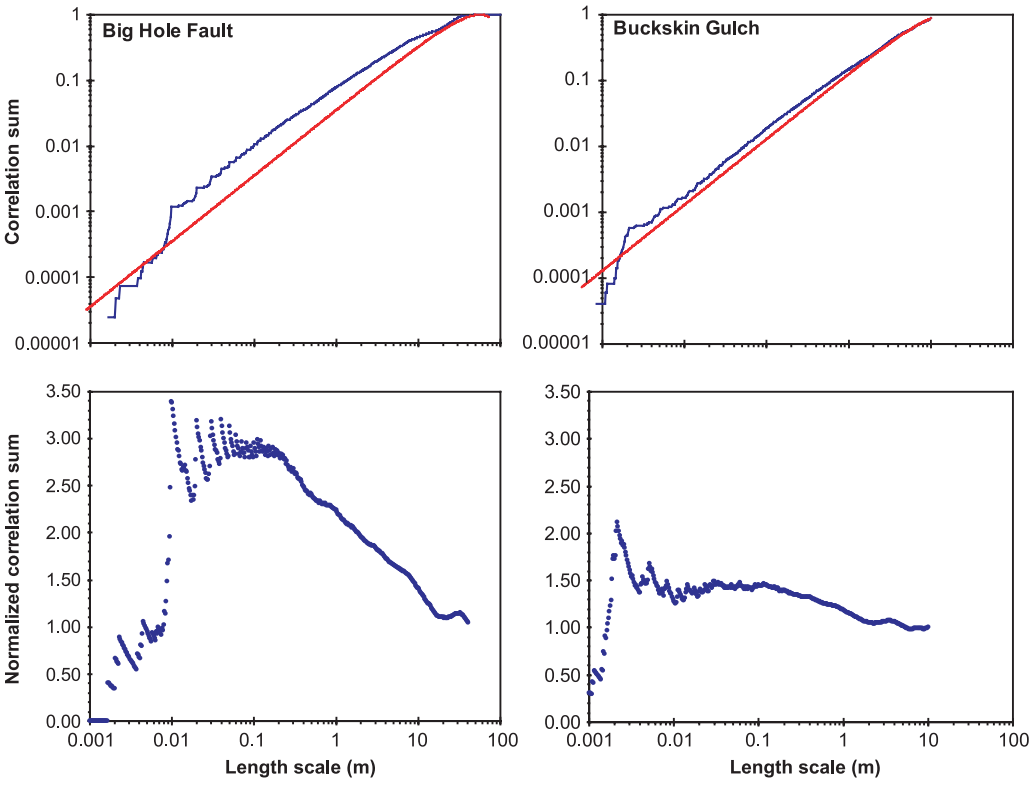

Figure 9. Plots of the correlation sum (upper panels) and normalized correlation sum (lower panels) for both locations. The red line on the upper panels shows the expected correlation sum for a random distribution (Gomez and Marrett, 2007). Note that the distribution from the Big Hole fault is more nonrandom than the distribution from Buckskin Gulch.

Band Permeabilities

Large hand samples (from ~25 to 2000 in.^{3} [410 to 32774 cm^3]) of rocks containing deformation bands were collected and wrapped in newspaper and duct tape to preserve them. These hand samples were sent to Core Lab in Houston, Texas, where multiple 1-in. (2.54-cm)-diameter plugs were collected from each sample. The plugs were drilled perpendicular to the dominant deformation-band orientation. Following drilling, the plugs were photographed and CT scanned. Visual inspection of the plugs and the CT scans were used to identify plugs that were free of coring-induced fractures and that contained well-defined band arrays. This subset of the plugs was selected for permeability measurements. Undeformed host-rock permeability was measured using a probe permeameter.

Band permeabilities were calculated using a harmonic averaging approach based on bulk air permeabilities of 2.54-cm (1-in.) plugs. Band thicknesses for the harmonic-averaging calculations were measured from high-resolution CT scans. Permeability measurements are summarized in Figure 10 and Table 3. Permeabilities of undeformed host rock are approximately 3300–7500 md (3.2×10^{-12} to 7.4×10^{-12} m^2 [34.4×10^{-12} to 79.6×10^{-12} ft^2]) at Buckskin Gulch and 660–1100 md (6.5×10^{-13} to 1.1×10^{-12} m^2 [69.9×10^{-13} to $11.8\ 10^{-12}$ ft^2]) at Big Hole. Shear band permeabilities at Buckskin Gulch range from 0.08 to 1.16 md ($0.08–1.14 \times 10^{-15}$ m^2 [$0.86–12.27 \times 10^{-15}$ ft^2]) with a mean permeability of 0.26 md (2.6×10^{-16} m^2 [27.9×10^{-16} ft^2]) or 4–5 orders of magnitude lower than undeformed host rock. A population of bed-parallel shear bands has a mean permeability of 555 md (5.5×10^{-15} m^2 [59.2×10^{-15} ft^2]) or 1 order of magnitude lower than undeformed host rock.

Permeability measurements of compaction bands failed because of the relatively unconsolidated nature of the samples that made collection of intact plugs for permeability measurements difficult. Shear bands at Valley of Fire, which as discussed above is an area that is similar to Buckskin Gulch, have an image-analysis-based permeability that is 3–5.5 orders of magnitude lower than undeformed host rock (Myers, 1999), comparable to the reductions measured in Buckskin Gulch samples using the combination of permeameter probe

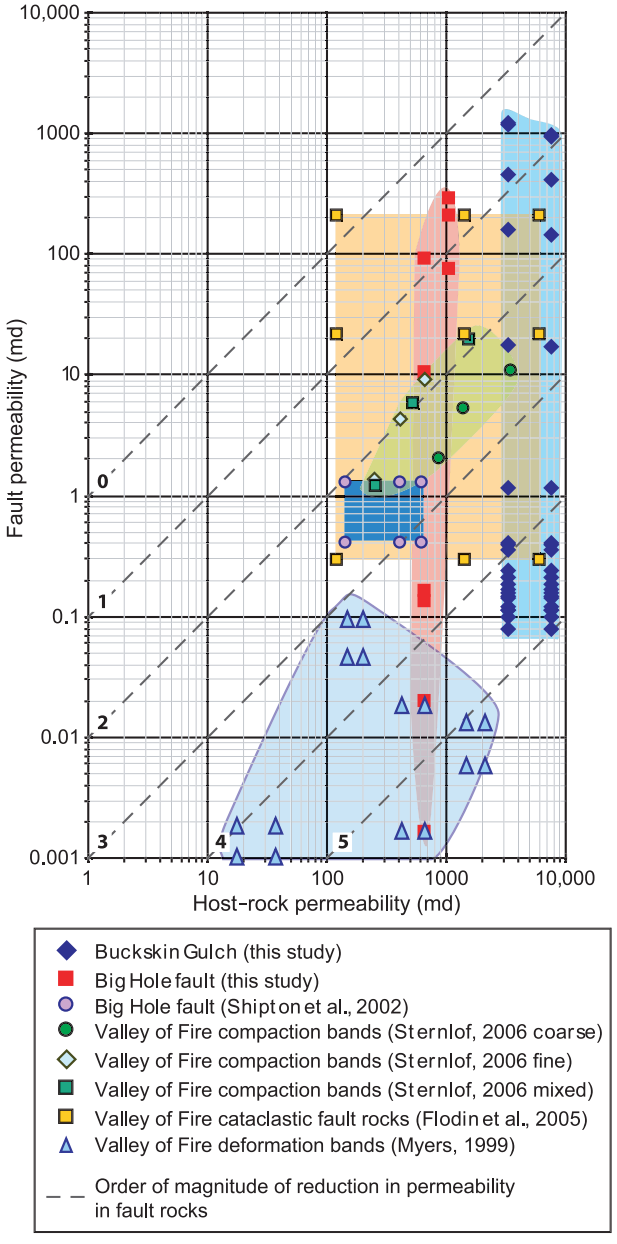

Figure 10. Compilation of host-rock and deformation-band permeability for Buckskin Gulch, the Big Hole fault, and the Valley of Fire.

measurements and whole-plug air permeability measurements described above. Image-analysis-based estimates of compaction band permeability at Valley of Fire show a reduction of 2–3 orders of magnitude relative to undeformed host rock. Individual image-based permeability measurements may be either higher or lower than whole-core-plug and probe measurements. However, Torabi and Fossen (2009) showed that this is because the image-based permeability measurements capture a wide range of heterogeneities that are not otherwise captured, and that on average, the image-based results are comparable to the other results. Consequently, because the reduction in permeability of the shear bands at Valley of Fire and Buckskin Gulch is similar, we assume that the reduction in permeability of the compaction bands is similar. Thus, we infer that the permeability of the compaction bands at Buckskin Gulch is 3.3–75 md ($0.3–7.4 \times 10^{-14}$ m^2 [$3.2–79.6 \times 10^{-14}$ ft^2]).

Shear bands at Big Hole have a median permeability of 0.13 md (1.3×10^{-16} m^2 [13.9×10^{-16} ft^2]), ranging from 0.002 to 10.6 md ($0.0002–1 \times 10^{-14}$ m^2 [$0.0021–10.7 \times 10^{-14}$ ft^2]). Note that median and not mean permeability is reported as one sample has a permeability of 10.6 md (1.04×10^{-14} m^2 [11.1×10^{-14} ft^2]), whereas the other four range from 0.002 to 0.16 md (2.0×10^{-18} to 1.6×10^{-16} m^2 [21.5×10^{-18} to 17.2×10^{-16} ft^2]). Therefore, the shear bands at Big Hole have a permeability reduction that is 3–5 times that of undeformed host rock. The median permeability is similar to the value of 0.4 md (3.9×10^{-16} m^2 [41.9×10^{-16} ft^2]) with a range of 0.4–1.3 md (3.9×10^{-16} to 1.3×10^{-15} m^2 [41.9×10^{-16} to 13.9×10^{-15} ft^2]) reported by Shipton et al (2002). Darker, noncataclastic bands at Big Hole have a permeability ranging from 75 to 285 md ($0.7–2.8 \times 10^{-13}$ m^2 [$7.5–30.1 \times 10^{-13}$ ft^2]) with an average of 164 md (1.6×10^{-13} m^2 [17.2×10^{-13} ft^2]).

Band Distributions and Effective Permeability

In general, faults and fractures display a size distribution that is similar to the band thickness distributions at Buckskin Gulch and at Big Hole (e.g., Marrett and Allmendinger, 1990, 1991). In the case of faults and fractures, the deviation at small sizes is interpreted to be the result of the undersampling of the population caused by a lack of resolution. In the case of deformation bands, this deviation is not a sampling artifact. Instead, because deformation bands cannot be infinitely thin, the lower limit on their thickness will be controlled

Table 3. Permeabilities of Protolith and Deformation Bands from Buckskin Gulch and the Big Hole Fault

	Average Permeability	Minimum Permeability	Maximum Permeability
Buckskin Gulch			
Protolith	5400 md (5.3×10^{-12} m^2)	3300 md (3.2×10^{-12} m^2)	7500 md (7.4×10^{-12} m^2)
Shear bands	0.26 md (2.6×10^{-16} m^2)	0.08 md (0.08×10^{-15} m^2)	1.16 md (1.14×10^{-15} m^2)
Compaction bands	39 md (3.9×10^{-14} m^2)	3.3 md (0.3×10^{-14} m^2)	75 md (7.4×10^{-14} m^2)
Big Hole Fault			
Protolith	880 md (8.8×10^{-13} m^2)	660 md (6.5×10^{-13} m^2)	1100 md (1.1×10^{-12} m^2)
Shear bands	0.13 md (1.3×10^{-16} m^2)	0.002 md (0.0002×10^{-14} m^2)	10.6 md (1×10^{-14} m^2)
Noncataclastic shear bands	164 md (1.6×10^{-13} m^2)	72 md (0.7×10^{-13} m^2)	285 md (2.8×10^{-13} m^2)

by grain size and failure mechanism. Individual band thickness should decrease with decreasing grain size and increasing cataclasis. The range of grain sizes from both field areas is shown on Figure 8. More of the population plots below the maximum grain-size thickness at Big Hole than at Buckskin, suggesting that cataclasis is a more important factor at Big Hole than at Buckskin. This is further supported by the observation that most of the bands from Buckskin Gulch are compaction bands with little cataclasis seen on photomicrographs (Mollema and Antonellini, 1996), whereas all of the bands at Big Hole are shear bands. Representative photomicrographs from the Buckskin Gulch and Big Hole locations showing shear bands, noncataclastic shear bands, and compaction bands are given in Figure 11.

The thickness distributions can be used to refine characterizations of band densities. Densities calculated from raw scan-line data do not take variations in band thickness into account, and therefore, bands with a thickness of 1 cm are given the same weight as bands with a thickness of 1 mm (0.03 in.). Because thicker bands form through the amalgamation of thinner bands (Aydin and Johnson, 1983), it is appropriate to treat thick bands as being composed of multiple thin bands when density distributions are calculated. The band-thickness distribution for Buckskin Gulch deviates from a power law at a thickness of about 1.0 mm (0.03 in.), whereas the equivalent deviation for Big Hole occurs at a value of about 0.35 mm (0.013 in.) (Figure 8). Because these deviations denote the smallest thickness for a self-similar band population, we use them to divide thicker bands into their thinner constituents. As seen on Figure 6, the maximum density for the unsplit bands at Buckskin Gulch is about 40 bands/m (~12 bands/ft) and about 24 bands/m (~7 bands/ft) at Big Hole despite the presence of several very thick bands at Big Hole (Figures 7, 8). Splitting the bands yields a maximum density of 92 1.0-mm-thick bands per meter (28 0.03-in.-thick bands per foot) for Buckskin Gulch and 228 0.35-mm-thick bands per meter (69 0.013-in.-thick bands per foot) at Big Hole. Figure 12 shows a moving average (1-m [3-ft] window calculated every 0.2 m [0.6 ft]) of band densities for split and unsplit band populations for both Buckskin Gulch and the Big Hole fault. As seen on Figure 12, the splitting process highlights trends, making them easier to interpret. The bands from Buckskin Gulch appear to occur in semiregularly spaced clusters with a spacing of about 3 m (10 ft). This value is similar to the fractal cluster spacing of 2.5 m (8.2 ft) inferred for these bands (discussed above, see also Figure 9). The splitting procedure highlights two zones of very thick bands (at 38 and 56.5 m [125 and 185.3 ft]) in the Big Hole data, which are not visible on the conventionally plotted data shown in Figure 6. As seen on Figure 12, the fault with a throw of 14 m (46 ft) is bound by an 18-m (59-ft)-wide zone of intense deformation bands. This value is similar to the fractal cluster spacing of 18 m (59 ft) inferred for this band population (Figure 9). This highlights some of the utility of performing a spatial analysis through calculation of the correlation sum/integral for scan-line data. Such an analysis provides a statistically rigorous estimate of

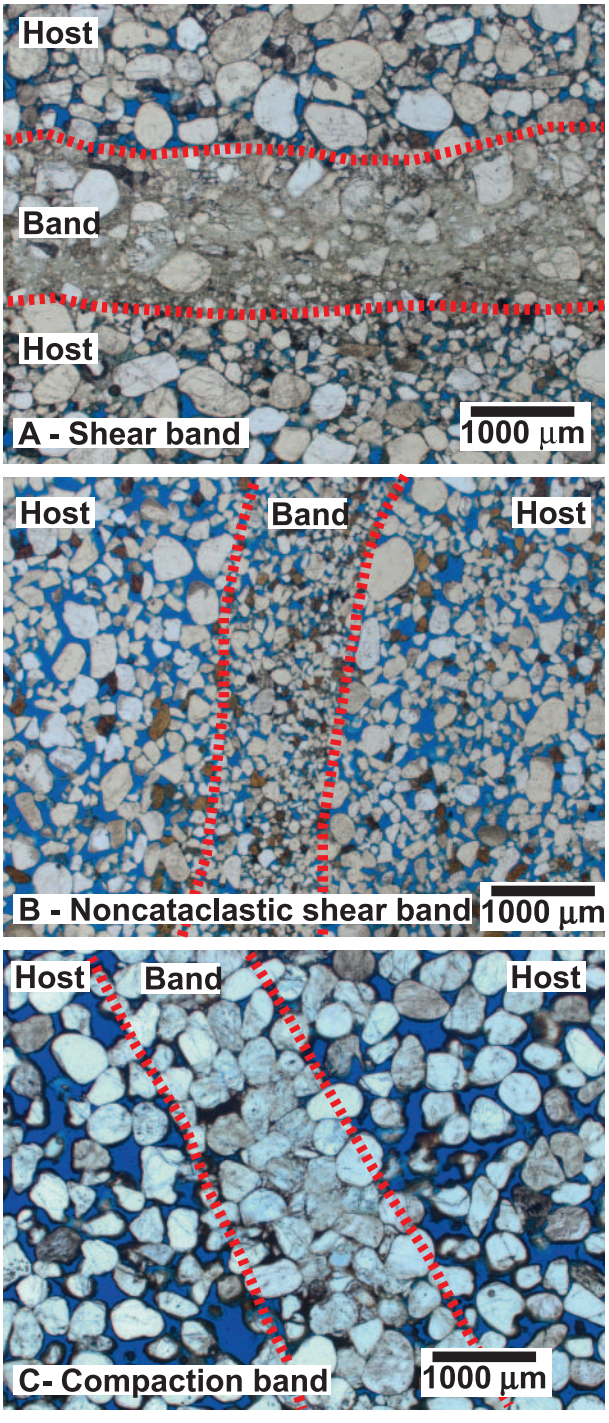

Figure 11. Representative photomicrographs of shear bands (A), noncataclastic shear bands (B), and compaction bands (C). Shear bands are observed at both Buckskin Gulch and the Big Hole fault, noncataclastic shear bands are observed at the Big Hole fault locality, and compaction bands are observed at the Buckskin Gulch location. Note that although all bands exhibit reduced porosity, and as shown in Table 3, reduced permeability, the degree of cataclasis is less in the noncataclastic shear band and compaction band relative to the shear band. The shear bands have the greatest reduction in permeability relative to undeformed host rock.

band-cluster spacing and damage-zone width and moreover provides insight into spatial characteristics that are not readily apparent on conventionally plotted graphs of band density such as those shown in Figure 6.

The deformation bands at the Big Hole fault location are related to regional stresses because they occur primarily in the damage zone of the Big Hole fault. The deformation bands at Buckskin Gulch are related to the regional stress as indicated by the following observations: (1) the shear bands at Buckskin Gulch occur in conjugate sets, with one set parallel to the fault that formed the east Kaibab monocline (Brandenburg et al., unpublished work); (2) the offsets along the shear bands are reverse, as is the regional stress state; (3) the compaction bands form normal to the greatest principal stress inferred for the monocline (Mollema and Antonellini, 1996). Possible explanations for the difference in the spatial distributions between the two sites include (1) differences in stress state, (2) differences in throw along the faults at Buckskin Gulch and Big Hole fault, and (3) difference in average band densities. The difference in throw along the faults and the difference in band densities can be discarded as possible reasons through comparison with an existing data set. Du Bernard et al. (2002) characterized the spatial distribution of deformation bands in the damage zone of normal faults in the Nubian sandstones in Egypt. The band densities from all of the locations described in that study are greater than either Buckskin Gulch and Big Hole, and as seen on Figure 13, the normalized correlation sums define a range that includes both Buckskin Gulch and Big Hole fault. This means that the more random nature of the spatial distribution at Buckskin Gulch is not due to the greater band density at that location because there are distributions from the Nubian sandstones that have a greater band density and a more highly nonrandom distribution than at Buckskin Gulch. Similarly, the greater throws along the faults at Big Hole are not likely to be responsible for the more nonrandom distribution at that location as the larger faults from the Nubian sandstones tend to have more random distributions (although this relationship is not perfect).

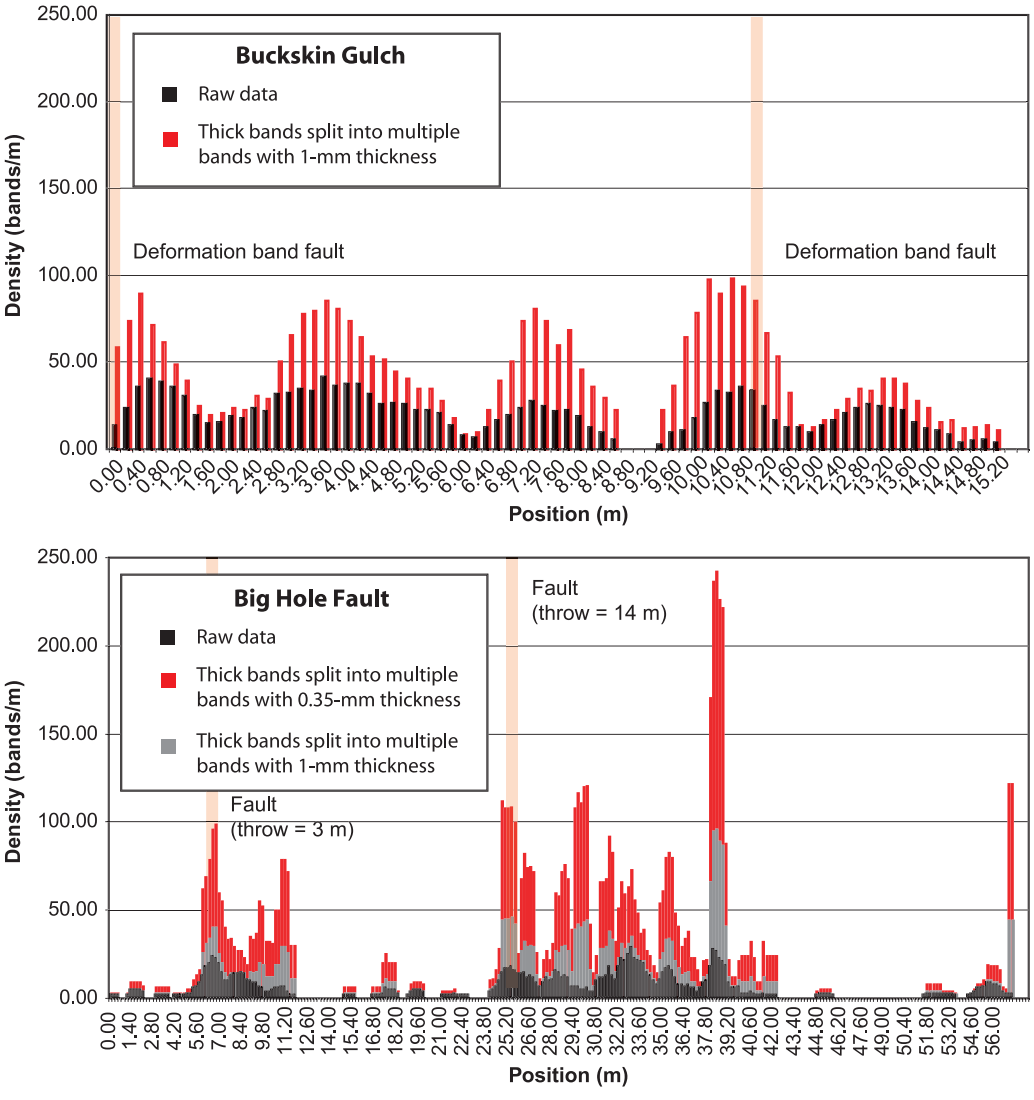

Figure 12. Deformation-band densities for Buckskin Gulch and the Big Hole fault calculated using a moving window average with a 1-m (3-ft) window. Raw band data are shown in black. Data sets in which thicker bands have been split into multiple thinner bands are shown in red and gray. This processes highlight the spatial distribution of the bands.

Effective Permeability

Constraining the thicknesses and spatial distributions of deformation bands allows effective permeability perpendicular to the bands to be calculated using harmonic averaging. Effective permeability can be calculated as

$$K_{\text{effective}} = \frac{T_{\text{total}}}{\frac{T_{\text{band}}}{K_{\text{band}}} + \frac{T_{\text{host}}}{K_{\text{host}}}} \qquad (2)$$

where $K_{\text{effective}}$ is the effective permeability, T_{total} is the total thickness (scan-line length), T_{band} is the cumulative thickness of the bands measured along the scan line, T_{host} is the cumulative thickness of undeformed host rock along the scan line, K_{band} is the band permeability, and K_{host} is the host-rock permeability. Input data for effective permeability calculations are given in Table 2. Assuming average host-rock, shear-band, and compaction-band permeabilities (Table 1), the effective permeability along the Buckskin Gulch scan line is 20 md (2.0×10^{-14} m^2 [21.5×10^{-14} m^2]), a reduction of 2.5 orders of magnitude with respect to undeformed host rock. Within the uncertainty of the input parameters, effective permeabilities for Buckskin Gulch range from 6 to 88 md (0.6–8.7×10^{-14} m^2 [6.4–93.6×10^{-14} ft^2]). Assuming average host-rock, shear-band, and noncataclastic-band permeabilities (Table 1), the effective permeability at Big Hole is 18 md (1.8×10^{-14} m^2 [19.3×10^{-14} ft^2]), a reduction of 1.7 orders of

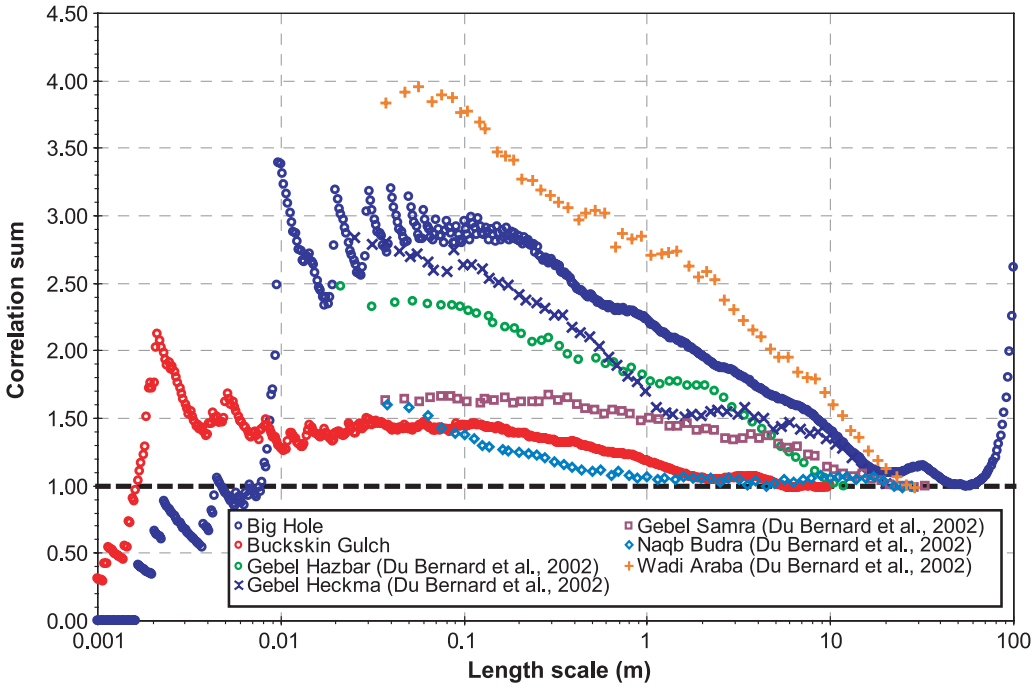

Figure 13. Compilation of correlation sum data for deformation-band occurrences. All of the localities from Du Bernard et al. (2002) are from deformation bands in the damage zones of normal faults.

magnitude with respect to undeformed host rock. The range of values for Big Hole effective permeabilities is from 0.3 to 23 md ($0.03–2.3 \times 10^{-14}$ m^2 [$0.32–24.7 \times 10^{-14}$ ft^2]), which is similar to the value of 30–40 md ($3.0–3.9 \times 10^{-14}$ m^2 [$32.2–41.9 \times 10^{-14}$ ft^2]) reported by Shipton et al. (2002).

As discussed above, the deformation-band occurrence at Big Hole occurs in conjunction with a small but seismically resolvable fault (throw up to 24 m [79 ft]). In contrast, the band occurrence at Buckskin Gulch occurs in conjunction with faults that are too small to have developed a slip surface. Assuming that deformation-band arrays evolve from isolated bands to amalgamations of bands to amalgamations of bands bounded by a throughgoing slip surface (Aydin, 1978), this means that the band array at Buckskin Gulch is less developed than the array at the Big Hole fault. Presumably if the deformation-band network at Buckskin Gulch had continued to develop, then eventually faults with throughgoing slip surfaces would have developed. This means that the reduction in effective permeability to approximately 20-md effective permeability occurred at an earlier stage of band-network evolution at Buckskin Gulch than at the Big Hole fault.

The band networks at Buckskin Gulch are up to a few tens of meters wide and up to approximately 200 m (656 ft) long. Based on mapping by Mollema (1994), they occur over an area of approximately 4 km^2 (1.5 mi^2). Whether networks of this size will cause compartmentalization will be controlled by whether it is possible for flow around the networks to occur. In structurally simple reservoirs with small numbers of distantly spaced deformation-band networks, the presence of Buckskin Gulch–style deformation-band networks is not likely to cause compartmentalization because flow pathways around the networks are possible. However, even in this simple case, the band arrays may reduce the recovery from the field because fluids will not be recovered from them. Moreover, in more structurally complex reservoirs with more and more closely spaced networks, the risk of compartmentalization increases as deformation-band networks may serve to bridge the gaps between networks, thereby preventing flow around them.

DISCUSSION

When the data concerning the spatial distributions of the bands are coupled with the effective permeability calculations, it appears that an effective

permeability-reducing array of deformation bands was more readily developed at Buckskin Gulch than along the Big Hole fault. The primary difference between the Buckskin Gulch and Big Hole fault localities is that the structures at Buckskin Gulch formed in a reverse-faulting environment at the edge of a Laramide fold (the East Kaibab monocline), whereas the structures at the Big Hole fault formed in a normal-faulting environment at the crest of a Laramide fold (the San Rafael swell). In terms of lithology, timing of deformation, and depth of deformation, the two locations are very similar. This is an indication that it is easier to form an effective permeability-reducing array of deformation bands in a reverse-faulting environment than it is in a normal-faulting environment.

Porosity, host-rock permeability, and grain size may also contribute to differences between the two sites, and so, placing Buckskin Gulch and the Big Hole fault in the context of the Navajo Sandstone as a whole is helpful. These parameters are given above but are summarized here. The mean grain size for undeformed host rock at Buckskin Gulch is 0.36 mm (0.013 in.) ranging from 0.09 to 0.6 mm (0.004 to 0.024 in.), a porosity of 20–23%, and an average permeability of 5400 md (5.3×10^{-12} m^2 [57×10^{-12} ft^2]) with a range of 3300–7500 md (3.3–7.4×10^{-12} m^2 [35.5–79.6×10^{-12} ft^2]). The mean grain size for undeformed host rock at the Big Hole fault is 0.17 mm (0.006 in.) ranging from 0.06 to 0.3 mm (0.002 to 0.01 in.), a porosity of 23–24% (Shipton et al., 2002), and an average permeability of 880 md (0.9×10^{-12} m^2 [9.6×10^{-12} ft^2) with a range of 660–1100 md (0.7–1.1×10^{-12} m^2 [7.5–11.8×10^{-12} ft^2]). Compiling data from Hood and Patterson (1984) in the northern San Rafael swell, the mean grain size for the Navajo is 0.15 mm (0.006 in.) with a range of 0.06 to 0.321 mm (0.002 to 0.01 in.), a mean porosity of 20% ranging from 4 to 29%, and a mean permeability of 710 md (7.0×10^{-13} m^2 [75.3×10^{-13} ft^2]) with a range of 13 to 3930 md (1.3×10^{-14} to 3.9×10^{-12} m^2 [13.9×10^{-14} to 41.9×10^{-12} ft^2]), excluding two samples (out of 20) with permeabilities of 0.02 and 0.03 md (2–3×10^{-17} m^2 [21.5–32.2×10^{-17} ft^2]). From these data, it appears that although Buckskin Gulch overlaps the range of values for the San Rafael swell, it generally exceeds them, which makes the supposition that the differences in band networks at Buckskin Gulch and at Big Hole are primarily caused by differences in stress state more difficult to verify. This difficulty is overcome to some extent when data from the Valley of Fire are considered. The Valley of Fire marks an occurrence of shear and compaction bands in the Aztec Sandstone (equivalent to the Navajo) that is similar to Buckskin Gulch. From the work of Flodin et al. (2005), the mean grain size at that location is 0.16 mm (0.006 in.) with a range of 0.05 to 0.33 mm (0.002–0.01 in.). The value of 0.05 mm (0.002 in.) is from a sample of host rock adjacent to a fault. and some is likely not representative of undeformed host rock. If that value is discarded, the minimum grain size is 0.16 mm (0.006 in.). The range of porosities is 15–25% (Flodin et al., 2005). Combining data from Myers (1999), Flodin et al. (2005), and Sternlof (2006), the average host-rock permeability at Valley of Fire is about 700 md (6.9×10^{-13} m^2 [74.2×10^{-13} ft^2]) with a range of 18–5991 md (1.8×10^{-14} to 5.9×10^{-12} m^2 [19.3×10^{-14} to 63.5×10^{-12} ft^2]). The range of grain size from Valley of Fire is compatible with the grain sizes from the Big Hole fault location, and as shown on Figure 10, an overlap in host-rock permeabilities also exists. This suggests that it is possible to form a Buckskin Gulch-type array in sandstones that have properties that are more representative of the average Navajo Sandstone in the San Rafael Swell. Note that compaction bands at Buckskin Gulch form preferentially in coarser dune sets (Mollema and Antonellini, 1996), but that most of the reduction in effective permeability is associated with the shear bands, which do not show lithologic control. Because of the localized nature of their occurrence, the density of compaction bands reported in this study represents the maximum extreme at Buckskin Gulch. However, because the shear bands are more broadly distributed through the study area and because they control the effective permeability, the effective permeabilities calculated above are generally applicable to Buckskin Gulch.

The differences in the band distributions and their resulting effect on permeability are therefore

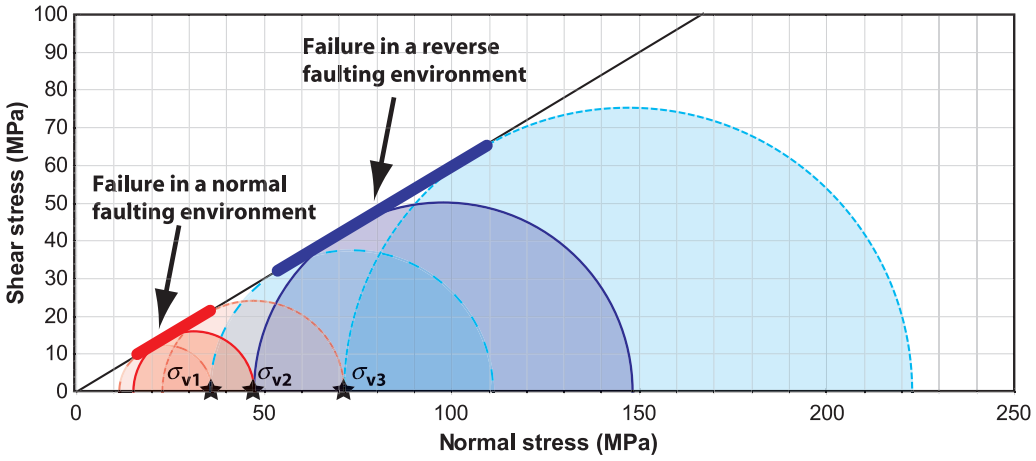

Figure 14. Stress states for Buckskin Gulch (blue) and Big Hole fault (red) assuming failure can be described using a Mohr-Coulomb failure criterion for burial depths of 1.5 (σ_{v1}), 2 (σ_{v2}), and 3 km (σ_{v3}) (0.9, 1.2, and 1.8 mi).

most likely due to differences in stress state at Buckskin Gulch and at Big Hole. Because shear bands at both sites exist and because the shear bands and compaction bands at Buckskin Gulch appear to be contemporaneous (Schultz, 2009) (Figure 4B), using a Mohr-Coulomb failure criterion to crudely estimate the stress state at each of those sites is appropriate because the Navajo Sandstone at both sites was experiencing shear failure. Assuming a burial depth of 2 km (1.2 mi), compatible with the depth estimates for both Buckskin Gulch and Big Hole discussed above, a mean dry density of 2.4 g/cm^3, and a hydrostatic fluid pressure, the effective vertical stress (σ_1 at Big Hole and σ_3 at Buckskin Gulch) would be approximately 28 MPa (4061 psi). Assuming a Byerlee's Law coefficient of friction of 0.6 (Byerlee, 1978), the mean and differential stresses at Buckskin Gulch would be 57 and 59 MPa (8267 and 8557 psi), and 18 and 19 MPa (2611 and 2756 psi) at Big Hole. The stress states for the two sites are summarized in Figure 14. Figure 14 shows that the range of mean stresses for Big Hole is 14–28 MPa (2030–4061 psi) as opposed to 43–85 MPa (6237–12,328 psi) at Buckskin Gulch. Because the primary difference between the two sites is the stress state, a thrust-faulting stress state applied to the same host rock appears to result in the creation of a network of deformation bands (shear and compaction bands) that has a greater reduction in effective permeability than if a normal-faulting stress state were applied to that same material. Furthermore, because compaction bands occur at Buckskin Gulch but not at Big Hole, the formation of compaction bands likely requires a thrust-faulting environment and therefore a higher mean and/or differential stress than for the formation of shear bands, which is compatible with earlier studies (Wong et al., 2004; Schultz and Siddharthan, 2005).

CONCLUSIONS

Despite general lithologic similarity, the effect of deformation-band arrays at Buckskin Gulch and at Big Hole Wash on reservoir permeability is greatly different on the reservoir scale. The average band-perpendicular effective permeability is approximately 18–20 md ($1.8–2.0 \times 10^{-14}$ m^2 [$19.3–21.5 \times 10^{-14}$ ft^2]) at both locations, but the development of a deformation-band array capable of causing that reduction is associated with a discrete fault-damage zone at the Big Hole fault. In contrast, the deformation-band arrays at Buckskin Gulch occur over a widespread area without any discrete faults except for the deformation-band faults, which likely have displacements on the order of tens of centimeters.

Because the deformation-band arrays at Buckskin Gulch formed under a thrust-faulting environment and the band arrays at the Big Hole fault formed in the same lithology at a similar depth and time in a normal-faulting environment, reducing effective permeability on a reservoir scale in a thrust-faulting environment is easier than in a normal-faulting environment (all other parameters held

constant). This means that the risk of reservoir degradation and potentially production time-scale compartmentalization by deformation bands is higher in thrust-faulting environments.

REFERENCES CITED

Antonellini, M., and A. Aydin, 1994, Effect of faulting on fluid flow in porous sandstones: Petrophysical properties: AAPG Bulletin, v. 78, no. 3, p. 355–377.

Antonellini, M., and A. Aydin, 1995, Effect of faulting on fluid flow in porous sandstones: Geometry and spatial distribution: AAPG Bulletin, v. 79, no. 5, p. 642–671.

Antonellini, M., A. Aydin, and L. Orr, 1999, Outcrop-aided characterization of a faulted hydrocarbon reservoir: Arroyo Grande oil field, California, U.S.A., *in* W. C. Haneberg, P. S. Mozley, J. C. Moore, and L. B. Goodwin, eds., Faults and subsurface flow in the shallow crust: American Geophysical Union Geophysical Monograph 113, p. 7–26.

Aydin, A., 1978, Small faults formed as deformation bands in sandstone: Pure and Applied Geophysics, v. 116, p. 913–930, doi:10.1007/BF00876546.

Aydin, A., and A. M. Johnson, 1983, Analysis of faulting in porous sandstones: Journal of Structural Geology, v. 5, no. 1, p. 19–31, doi:10.1016/0191-8141(83)90004-4.

Aydin, A., R. I. Borja, and P. Eichubl, 2006, Geological and mathematical framework for failure modes in granular rock: Journal of Structural Geology, v. 28, p. 83–98, doi:10.1016/j.jsg.2005.07.008.

Beach, A., A. I. Welbon, P. J. Brockbank, and J. E. McCallum, 1999, Reservoir damage around faults: Outcrop examples from the Suez Rift: Petroleum Geosciences, v. 5, p. 109–116.

Beitler, B., W. T. Parry, and M. A. Chan, 2005, Fingerprints of fluid flow: Chemical diagenetic history of the Jurassic Navajo Sandstone, southern Utah, U.S.A.: Journal of Sedimentary Research, v. 75, p. 547–561, doi:10.2110/jsr.2005.045.

Berg, S. S., and T. Skar, 2005, Controls on damage zone asymmetry of a normal fault zone: Outcrop analysis of a segment of the Moab fault, SE Utah: Journal of Structural Geology, v. 27, p. 1803–1822, doi:10.1016/j.jsg.2005.04.012.

Bohannon, R. G., 1983, Geologic map, tectonic map and structure sections of the Muddy and northern Black Mountains, Clark County, Nevada: U.S. Geological Survey map I-1406, scale 1:62,500, 2 sheets.

Byerlee, J., 1978, Friction of rocks: Pure and Applied Geophysics, v. 166, p. 615–625, doi:10.1007/BF00876528.

Cashman, S., and K. Cashman, 2000, Cataclasis and deformation-band formation in unconsolidated marine terrace sand, Humboldt County, California: Geology, v. 28, no. 2, p. 111–114, doi:10.1130/0091-7613(2000)28<111:CADFIU>2.0.CO;2.

Cifelli, R. L., 1990, Cretaceous mammals of southern Utah, I, Marsupials from the Kaiparowits Formation (Judithian): Journal of Vertebrate Paleontology, v. 10, no. 2, p. 295–319.

Davatzes, N. C., A. Aydin, and P. Eichhubl, 2003, Overprinting faulting mechanisms during the development of multiple fault sets, Chimney Rock fault array, Utah: Tectonophysics, v. 363, p. 1–18, doi:10.1016/S0040-1951(02)00647-9.

Davis, G. H., 1978, Monocline fold pattern of the Colorado Plateau, *in* V. Matthews, ed., Laramide folding associated with basement block faulting in the western United States: Geological Society of America Memoir 151, p. 215–233.

Davis, G. H., 1999, Structural geology of the Colorado Plateau region of southern Utah, with special emphasis on deformation bands: Geological Society of America Special Paper 342, 157 p.

Davis, G. H., A. P. Bump, P. E. Garcia, and S. G. Ahlgren, 1999, Conjugate Reidel deformation band shear zones: Journal of Structural Geology, v. 22, p. 169–190, doi:10.1016/S0191-8141(99)00140-6.

Dickinson, W. R., and G. E. Gehrels, 2009, U-Pb ages of detrital zircons in Jurassic eolian and associated sandstones of the Colorado Plateau: Evidence for transcontinental dispersal and intraregional recycling of sediment: Geological Society of America Bulletin, v. 121, no. 3/4, p. 408–433.

Doelling, H. H., and F. D. Davis, 1989, Geology of Kane County, Utah: Utah Geological and Mineral Survey map 121, scale 1:100,000, 10 sheets.

Du Bernard, X., P. Labaume, C. Darcel, P. Davy, and O. Bour, 2002, Cataclastic slip band distribution in normal fault damage zones, Nubian sandstones, Suez rift: Journal of Geophysical Research, v. 107, p. 2141, doi:10.1029/2001JB000493.

Eichubl, P., W. L. Taylor, D. D. Pollard, and A. Aydin, 2004, Paleo-fluid flow and deformation in the Aztec Sandstone at the Valley of Fire, Nevada—Evidence for the coupling of hydrogeologic, diagenetic, and tectonic processes: Geological Society of America Bulletin, v. 116, no. 9/10, p. 1120–1136, doi:10.1130/B25446.

Engebretson, D. C., A. Cox, and G. A. Thompson, 1984, Correlation of plate motions with continental tectonics: Laramide to Basin-Range: Tectonics, v. 3, p. 115–119, doi:10.1029/TC003i002p00115.

Flodin, E., M. Prasad, and A. Aydin, 2003, Petrophysical constraints on deformation styles in Aztec Sandstone, southern Nevada, U.S.A.: Pure and Applied Geophysics, v. 160, p. 1589–1610.

Flodin, E., M. Gerdes, A. Aydin, and W. D. Wiggins, 2005, Petrophysical properties and sealing capacity of fault rock, Aztec Sandstone, Nevada, *in* R. Sorkhabi and Y. Tsuji, eds., Fault, fluid flow and petroleum traps: AAPG Memoir 85, p. 197–217.

Fossen, H., and J. Hesthammer, 1998, Deformation bands and their significance in porous sandstone reservoirs: First Break, v. 16, p. 21–25, doi:10.1046/j.1365-2397.1998.00683.x.

Fossen, H., J. Hesthammer, T. E. S. Johansen, and T. O. Sygnabere, 2003, Structural geology of the Huldra field, northern North Sea—A major tilted fault block at the

eastern edge of the Horda platform: Marine and Petroleum Geology, v. 20, no. 10, p. 1105–1118, doi:10.1016/j.marpetgeo.2003.07.003.

Fossen, H., T. Erlend, S. Johansen, J. Hesthammer, and A. Rotevatn, 2005, Fault interaction in porous sandstone and implications for reservoir management, examples from southern Utah: AAPG Bulletin, v. 89, no. 12, p. 1593–1606, doi:10.1306/07290505041.

Fossen, H., R. A. Schultz, Z. K. Shipton, and K. Mair, 2007, Deformation bands in sandstone: A review: Journal of the Geological Society (London), v. 164, p. 755–769, doi:10.1144/0016-76492006-036.

Fowles, J., and S. Burley, 1994, Textural and permeability characteristics of faulted, high porosity sandstones: Marine and Petroleum Geology, v. 11, no. 5, p. 608–623, doi:10.1016/0264-8172(94)90071-X.

Gibson, R. G., 1994, Fault-zone seals in siliciclastic strata of the Columbus Basin, offshore Trinidad: AAPG Bulletin, v. 78, no. 9, p. 1372–1385.

Gomez, L., and R. Marrett, 2007, Diagenetic controls on spatial arrangement of fractures: An example from the Cupido F., Sierra Madre Oriental, Mexico: AAPG Annual Meeting Abstracts, http://www.searchanddiscovery.net/abstracts/html/2007/annual/index.htm (accessed July 2009).

Hesthammer, J., P. A. Bjørkum, and L. Watts, 2002, The effect of temperature on sealing capacity of faults in sandstone reservoirs: Examples from the Gullfaks and Gullfaks Sør fields, North Sea: AAPG Bulletin, v. 86, no. 10, p. 1733–1751.

Hood, J. W., and D. J. Patterson, 1984, Bedrock aquifers in the northern San Rafael swell area, Utah, with special emphasis on the Navajo Sandstone: State of Utah Department of Natural Resources Technical Publication 78, 128 p.

Knott, S. D., A. Beach, P. J. Brockbank, J. L. Brown, J. E. McCallum, and A. I. Welbon, 1996, Spatial and mechanical controls on normal fault populations: Journal of Structural Geology, v. 18, p. 359–372, doi:10.1016/S0191-8141(96)80056-3.

Krantz, M., 1988, Multiple fault sets and three-dimensional strain: Theory and application: Journal of Structural Geology, v. 10, p. 225–237, doi:10.1016/0191-8141(88)90056-9.

Leveille, G. P., R. Knipe, C. More, D. Ellis, G. Dudley, G. Jones, Q. J. Fisher, and G. Allinson, 1997, Compartmentalization of Rotliegendes gas reservoirs by sealing faults, Jupiter fields area, southern North Sea, *in* K. Ziegler, P. Turner, and S. R. Daines, eds., Petroleum geology of the southern North Sea: Future potential: Geological Society (London) Special Publication 123, p. 87–104.

Lewis, H., and G. D. Couples, 1993, Production evidence for geological heterogeneities in the Anschutz Ranch East field, western U.S.A., *in* C. P. North and D. J. Prosser, eds., Characterization of fluvial and eolian reservoirs: Geological Society (London) Special Publication 73, p. 321–338.

Marrett, R., and R. W. Allmendinger, 1990, Kinematic analysis of fault-slip data: Journal of Structural Geology, v. 12, p. 973–986, doi:10.1016/0191-8141(90)90093-E.

Marrett, R., and R. W. Allmendinger, 1991, Estimates of strain due to brittle faulting: Samples of fault populations: Journal of Structural Geology, v. 13, p. 735–738, doi:10.1016/0191-8141(91)90034-G.

Marzolf, J. E., 1983, Changing wind and hydrologic regimes during deposition of the Navajo and Aztec sandstones, Jurassic (?), southwestern United States, *in* M. E. Brookfield and T. S. Ahlbrandt, eds., Eolian sediments and processes: Guelph, Ontario, University of Guelph, p. 635–660.

Mollema, P. N., 1994, The influence of structural position and lithology on the fracture distribution in the East Kaibab monocline, SE Utah: Implications for fluid flow properties: Master's thesis, Stanford University, Palo Alto, California, 80 p.

Mollema, P. N., and M. A. Antonellini, 1996, Compaction bands: A structural analog for anti-mode I cracks in eolian sandstone: Tectonophysics, v. 267, p. 209–228, doi:10.1016/S0040-1951(96)00098-4.

Myers, R. D., 1999, Structure and hydraulics of brittle faults in sandstone: Ph.D. dissertation, Stanford University, Palo Alto, California, 176 p.

Nichols, D. J., 1997, Palynology and ages of some Upper Cretaceous formations in the Markagunt and northwestern Kaiparowits plateaus, southwestern Utah, *in* F. Maldonado and L. D. Nealey, eds., Geologic studies in the Basin and Range-Colorado Plateau transition in southeastern Nevada, southwestern Utah, and northwestern Arizona, 1995: U.S. Geological Survey Bulletin 2153-E, p. 79–106.

Parnell, J., G. R. Watt, D. Middleton, J. Kelly, and M. Baron, 2004, Deformation band control on hydrocarbon migration: Journal of Sedimentary Research, v. 74, no. 4, p. 552–560, doi:10.1306/121703740552.

Pittman, E. D., 1981, Effect of fault-related granulation on porosity and permeability of quartz sandstones, Simpson Group (Ordovician), Oklahoma: AAPG Bulletin, v. 65, no. 11, p. 2381–2387.

Schultz, R. A., 2009, Scaling and paleodepth of compaction bands, Nevada and Utah: Journal of Geophysical Research, v. 114, p. B03407, doi:10.1029/2008JB005876.

Schultz, R. A., and C. M. Balasko, 2003, Growth of deformation bands into echelon and ladder geometries: Geophysical Research Letters, v. 30, p. 2033, doi:10.1029/2003GL018449.

Schultz, R. A., and H. Fossen, 2008, Terminology for structural discontinuities: AAPG Bulletin, v. 92, no. 7, p. 853–867, doi:10.1306/02200807065.

Schultz, R. A., and R. Siddharthan, 2005, A general framework for the occurrence and faulting of deformation bands in porous granular rocks: Tectonophysics, v. 411, p. 1–18.

Shipton, Z. K., and P. A. Cowie, 2001, Damage zone and slip-surface evolution over [micrometer] to km scales in high-porosity Navajo Sandstone, Utah: Journal of Structural Geology, v. 23, p. 1825–1844, doi:10.1016/S0191-8141(01)00035-9.

Shipton, Z. K., J. P. Evans, K. R. Robeson, C. B. Forster, and S. Snelgrove, 2002, Structural heterogeneity and permeability in faulted eolian sandstone: Implications for

subsurface modeling of faults: AAPG Bulletin, v. 86, no. 5, p. 863–883.
Shipton, Z. K., J. P. Evans, and L. B. Thompson, 2005, The geometry and thickness of deformation-band fault core and its influence on sealing characteristics of deformation-band fault zones, *in* R. Sorkhabi and Y. Tsuji, eds., Faults, fluid flow and petroleum traps: AAPG Memoir 85, p. 181–195.
Sternlof, K. R., 2006, Structural geology, propagation mechanics and hydraulic effects of compaction bands in sandstone: Ph.D. dissertation, Stanford University, Palo Alto, California, 214 p.
Sternlof, K. R., J. W. Rudnicki, and D. D. Pollard, 2005, Anticrack inclusion model for compaction bands in sandstone: Journal of Geophysical Research, v. 110, p. B11403, doi:10.1029/2005JB003764.
Taylor, W. L., and D. D. Pollard, 2000, Estimation of in situ permeability of deformation bands in porous sandstone, Valley of Fire, Nevada: Water Resources Research, v. 36, no. 9, p. 2595–2606, doi:10.1029/2000WR900120.
Tindall, S. E., and G. H. Davis, 1999, Monocline development by oblique-slip fault-propagation folding: The east Kaibab monocline, Colorado Plateau, Utah: Journal of Structural Geology, v. 21, p. 1303–1320, doi:10.1016/S0191-8141(99)00089-9.
Torabi, A., and H. Fossen, 2009, Spatial variation of microstructure and petrophysical properties along deformation bands in reservoir sandstones: AAPG Bulletin, v. 93, no. 7, p. 919–938, doi:10.1306/03270908161.
Troyer, R., A. P. Barth, J. L. Wooden, and C. Jacobsen, 2006, Provenance and timing of Sevier foreland basin sediments in the Valley of Fire, southern Nevada, from U-Pb geochronology (abs.): Geological Society of America Abstracts with Programs, v. 38, p. 369.
Underhill, J. R., and N. H. Woodcock, 1987, Faulting mechanisms in high-porosity sandstones, New Red Sandstone, Arran, Scotland, *in* M. E. Jones and R. M. F. Preston, eds., Deformation of sediments and sedimentary rocks: Geological Society Special Publication 29, p. 91–105.
Utah State Geographic Information Database, 2010, http://gis.utah.gov/sgid (accessed March 1, 2008).
Witkind, I. J., 1988, Geologic map of the Huntington 30' × 60' quadrangle, Carbon, Emery, Grand, and Uintah counties, Utah: U.S. Geological Survey Map I-1764, scale 1:100,000, 1 sheet.
Wong, T.-F., C. David, and B. Menéndez, 2004, Mechanical compaction, *in* Y. Guéguen and M. Boutéca, eds., Mechanics of fluid-saturated rocks: International Geophysics Series: Amsterdam, Elsevier, v. 89, p. 55–114.